POLITECNICO DI TORINO

Master of science in Electronic engineering

Master degree Thesis

Nouvelle génération de sources de temps pour la technologie 5G

Academic tutor:

Prof. Danilo DEMARCHI

Author:

Mohamed Khalil JEMNI

Company tutors:

Dr. Marc SANSA PERNA

Dr. Bruno REIG

September 2019

ABSTRACT

In the last years, microelectromechanical systems (MEMS) have become ubiquitous components in a large number of commercial products. Thanks to their excellent features like small size, high quality factors at high frequencies, low fabrication cost and the possibility to be co-integrated with CMOS IC technology, MEMS resonators have shown significant abilities for sensing and high frequency signal processing applications. In the field of time references, they represent an alternative to current quartz crystal technology that has reached its limits with persistent drawbacks like a relatively large size, high cost and low compatibility with IC chips.

The aim of this internship is to start the development of time references based on MEMS resonators for 5G applications. This document starts with a general study of MEMS resonators, specifically of those developed in CEA-LETI. Then it follows with the RF characterization of these resonators, which allowed to extract their main performance indicators. The third part of the document treats time references based on MEMS resonators, which comprises a theoretical introduction and the design of an oscillator adapted to one of the measured devices. The last part of the document comprises a broad state of the art covering MEMS resonators and time references, with a special focus on MEMS time references.

Acknowledgement

This thesis internship becomes a reality thanks to the support and help of many individuals. I would like to extend my sincere acknowledgement to all of them.

I would like to express my special thanks of gratitude to my supervisor, doctor Marc SANSA PERNA and my second supervisor, doctor Bruno REIG who gave me the golden opportunity to do this wonderful thesis internship in such prestigious establishment. I want to thank them for their insightful conversations during the development of the ideas in this master thesis and for their helpful comments.

I would also like to thank my ENSIL-ENSCI and POLITECNICO DI TORINO professors and CEA-LETI experts who have offered me guidance, feedbacks and suggestions during my double degree cursus and my internship.

I want to express my deep gratitude to my parents for their love and support throughout my life. Thank you for your support and encouragement in many moments of crisis. My sisters, aunties, uncles, cousins deserve my wholehearted thanks as well.

To all my friends, thank you for the amazing time we passed together, your friendship makes my life a wonderful experience, I cannot list all of you here, but you are always in my heart.

I could not have done any of this without you. Thank you all.

Table of contents

Index of Figures

Index of Tables

1 Company introduction

*CEA

The Commissariat for Atomic Energy and Alternative Energy (CEA) is a public scientific, technical and industrial research organization (EPIC). A major player in research, development and innovation, CEA is active in four areas: defense and security, low carbon energy (nuclear and renewable), technological research for industry and fundamental research. Based on its recognized expertise, CEA participates in the implementation of collaborative projects with numerous academic and industrial partners.

The CEA is established in 9 centers all over France. It develops numerous partnerships with other research organizations, local communities and universities. As such, the CEA is involved in national alliances coordinating French research in the fields of energy (ANCRE), life sciences and health (AVIESAN), digital sciences and technologies (ALLISTENE), Environmental Sciences (AllEnvi) and Humanities and Social Sciences (ATHENA). Recognized as an expert in its fields of expertise, the CEA is fully integrated in the European Research Area and has a growing presence at the international level. The CEA is the only French research organization to be included in the Clarivate 2018 ranking and is the 2nd largest French patent filer in Europe, according to the European Patent Office (EPO) 2018 ranking.

The DRT is the Technological Research division of the CEA. It is organized around its three institutes specializing in micro and nanotechnologies (LETI), software-based systems (LIST) and new energy and nanomaterials technologies (LITEN).

CEA Tech is the technology research branch of the French Alternative Energies and Atomic Energy Commission (CEA), a key player in research, development and innovation in defense & security, nuclear energy, technological research for industry and fundamental physical and life sciences. In 2015, Thomson Reuters identified CEA as the most innovative research organization in the world.

*CEA-LETI

It is a technology research institute pertaining to the CEA focuses in micro and nanotechnologies, tailoring differentiating applicative solutions that ensure competitiveness in a wide range of markets. The institute tackles critical challenges such as healthcare, energy, transport and ICTs. Its multidisciplinary teams deliver solid expertise for applications ranging from sensors to data processing and computing solutions, leveraging world-class pre-industrialization facilities.

LETI builds long-term relationships with its industrial partners - global companies, SMEs and startups – and actively supports the launch of technology startups, being one of the most prolific research institutes in the world in terms of technological start-ups: SOITEC, SOFRADIR, ULIS, MOVEA, APIX Technology, HELIODEL and others in the making ... LETI is a member of the Carnot Institutes network.

LETI's main divisions are:

- Architecture and IC design, embedded software
- Silicon components
- Silicon technologies
- Optics and Photonics

- Technologies for Biology and Health
- Systems and solutions integration

Figure 1.1 : Key dates and statistics of LETI shows some statistics and key dates about LETI:

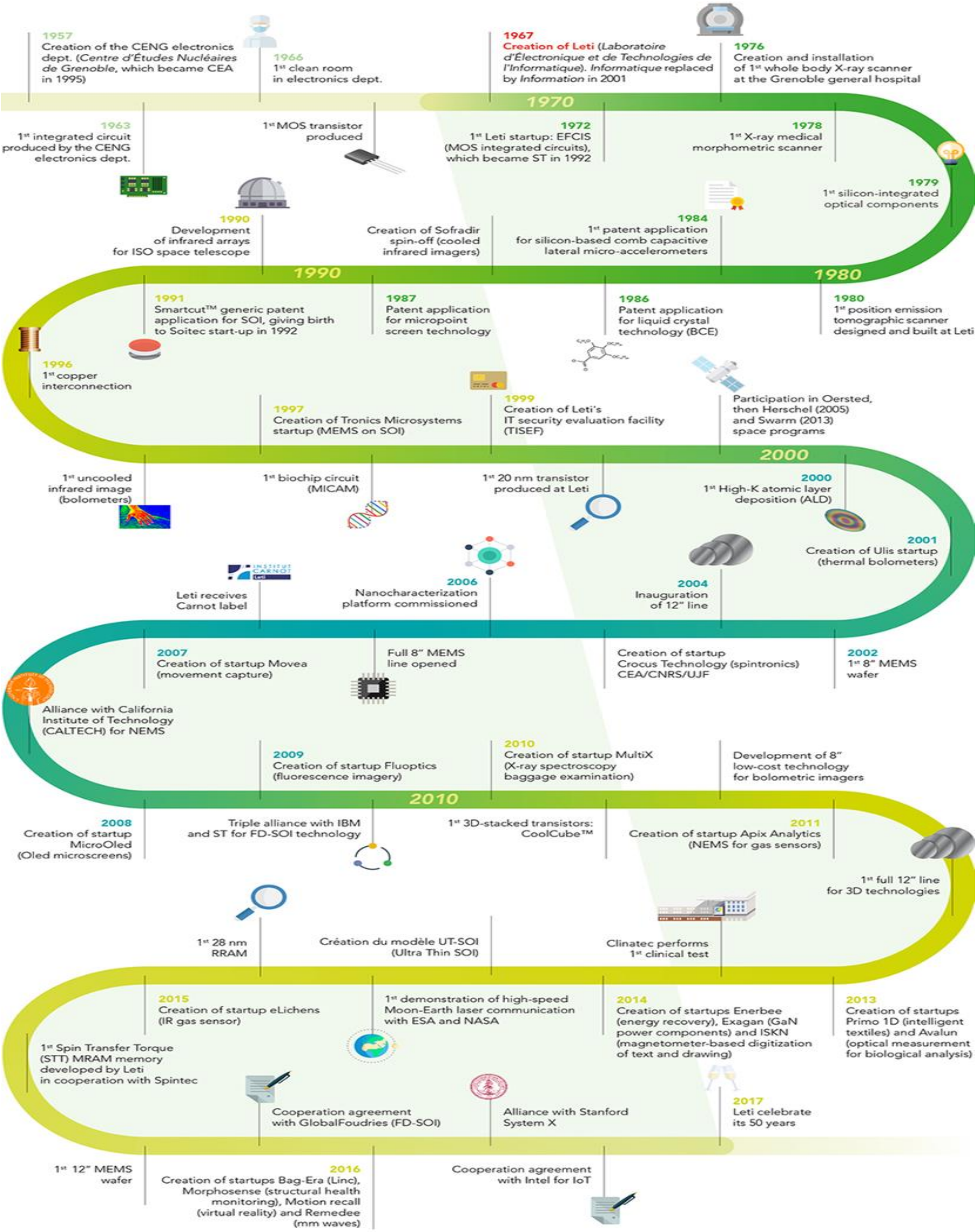

Figure 1.1 : Key dates and statistics of LETI

I performed my internship in the Radio-frequency components laboratory (French acronym: LCRF). It is a part of the service for power and energy (French acronym: SCPE) which is a part of the Silicon Components division. The LCRF main work consists of developing innovative radio frequency components, especially for “More Than Moore” applications, comprising materials, silicon integration, RF MEMS and passive components prototyping.

**Sustainable development

The CEA places sustainable development at the heart of its R&D programs, in a responsible corporate approach. The organization contributes to progress through knowledge and technology, is committed to reduce the environmental footprint of its activities and adheres to the values of social responsibility among its employees and stakeholders. It acts for economic development while ensuring the transparency of its activities through openness and dialogue. Attentive to its environment, controlling its energy consumption and preserving biodiversity, the CEA is an essential player in the development of technologies that will contribute to France's contribution to the 14 sustainable development objectives of the UN Agenda 2030.
At the Grenoble site, the CEA has set up hydrogen production by electrolysis of water, using electricity from renewable sources and metal hydride storage technologies developed in its research laboratories. This production supplies an external vehicle station and the clean room laboratories dedicated to Leti's microelectronics.

**Health/Safety

The Laboratory of Medical Biology (LBM) of the CEA/Grenoble is a laboratory dedicated to occupational health, it is therefore in charge of carrying out the medical biology examinations prescribed by occupational physicians, in accordance with the regulations in force.
As a "classic" medical laboratory, it performs the following tasks:
-Patient reception
-Transmission of information for the proper performance of sampling and examinations
-Sampling with the collection of relevant clinical data
-Consulting services
Since 2010, in parallel with its "traditional" laboratory activities, the LBM has developed an R&D activity focused on the development of biomarkers of exposure or effects of people potentially exposed to nanoparticles. Thus, the LBM is looking for biomarkers of early exposure and effect to this type of product.

2 General introduction

Clocks (reference oscillators) are ubiquitous components in electronic circuits: they are used as a time reference, to control data transmission in digital protocols, as RF signals modulators… The arrival of new technologies such as 5G or autonomous vehicles require performances that are extremely difficult to reach with current commercial technologies. In particular, 5G technology requires high-performance time sources with frequencies up to tens of GHz.

Reference oscillators based on Micro-Electro-Mechanical Systems (MEMS) are an emerging class of highly miniaturized, batch manufacturable timing devices that can surpass the performance of well-established quartz-based oscillators, especially at high frequencies. The MEMS resonators at the heart of this technology are the key component determining the reference oscillator's performance. Therefore, it is important to develop and optimize high-performance MEMS resonators in the GHz range to target 5G applications.

My internship consisted in performing the first steps towards the development of MEMS resonators for reference oscillators in the 5G technology. With this objective, I first performed a general study of MEMS resonators and their key parameters, which allowed me to familiarize with this multi-disciplinary field which mixes electronics, physics and mechanics. Then I proceeded to characterize some MEMS resonators fabricated at CEA-LETI, and extracted some of the important parameters for reference oscillator applications. Based on these measurements I implemented a standard model of the resonators into MATLAB software and I suggested a model of an oscillator. I finished with a state of the art of MEMS resonators and clocks in the GHz range, which allowed me to identify the most promising technologies and compare the CEA-LETI's devices with other technologies.

3 Introduction to MEMS resonators

Nowadays, MEMS resonators are generating significant research and commercial interest because of their numerous and high impact applications. Apart from timing applications, these resonant elements are used for sensing or filtering applications. This chapter introduces the concept of MEMS resonators, their operation techniques and their equivalent electrical model.

First, it is essential to define resonance and resonator. An object free to vibrate tends to do so at a specific rate called the object's natural, or resonant, frequency. (This frequency depends on the size, shape, and composition of the object.) Such an object will vibrate strongly when it is subjected to vibrations or regular impulses at a frequency equal to or very close to its natural frequency, this phenomenon is called resonance.

3.1 Types of MEMS resonators

MEMS resonators are composed of two parts: a mechanical part and an electrical part. These devices comprise a mechanical element in the micrometer scale and transducers which allow converting its mechanical motion into electrical signals and vice versa. The mechanical part of the resonator is the vibrating element. The transduction provides actuation of the mechanical structures, as well as a means to detect their vibration. For example, applying an electrical signal to an electrode dedicated to the actuation results in a mechanical excitation of the resonant structure: we speak about an electro-mechanical transduction. Similar principles can be applied to detection, resulting in a reverse (mechanical-electrical) transduction. To do this, we can consider different methods, some of them are cited in later sections.

MEMS resonators can be divided in two main categories, depending on the origin of their mechanical resonance: vibration-mode resonators and acoustic wave resonators (Figure 3.1).

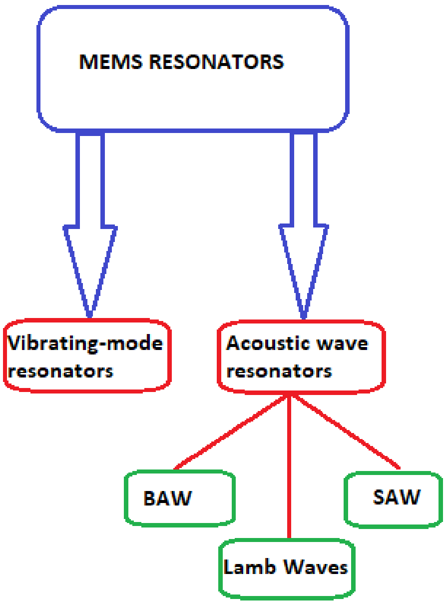

Figure 3.1 : Summary of MEMS resonators types

The first category of resonators is based on the vibration of a finite and generally released mechanical structure and is composed of different families: vibrating beams, longitudinal beams, bulk square extensional plates, elliptic or contour mode disks or rings, among others.

Cantilevers are probably the most common vibrating-mode resonators. As an example, we can consider a vibrating beam with a length L and a thickness h (Figure 3.2). Generally, the vibrating beam is biased with a

DC voltage V_p. When an oscillating signal is applied to the resonator at the fixed electrode (activation), the vibrating beam presents a maximum of displacement d_0 at the resonance frequency f_r. These displacements induces capacity C variations that are detected by the same fixed electrode (output).

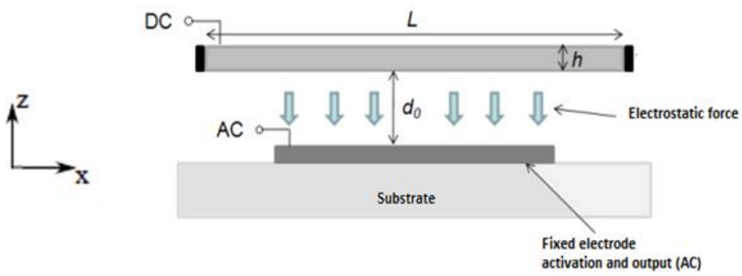

Figure 3.2 : Schematic an electromechanical resonator based on a vibrating beam

While vibrating-mode resonators use a beam or a disk, acoustic wave resonators are based on the sound-like waves propagating in a solid material. They exploit the piezoelectric properties of materials such as AlN or ZnO. These piezoelectric resonators can be classified into three subgroups according to their principle of operation: surface acoustic wave resonators (SAW), bulk acoustic wave (BAW) resonators and Lamb wave resonators (LWR). An acoustic wave can indeed propagate in solid materials following two types of waveforms: a longitudinal wave where particle movements occurs in the direction of the wave propagation and a shear wave where the movement of the particles is in a direction transverse to the direction of the spread. Waves propagating in an infinite[1] piezoelectric material are called volume acoustic waves. If the environment has limits, the waves are confined in a cavity governed by certain boundary conditions, causing wave reflections. In that case, interference of such waves gives birth to a resonance. These boundary conditions can introduce additional types of waves such as Rayleigh waves propagating at the free surface of the piezoelectric material, which correspond to surface acoustic waves (SAW).

3.2 Parameters of MEMS resonators

3.2.1 Resonance frequency

Generally, resonance occurs when a structural system is forced at a frequency corresponding to one of the natural frequencies of the system. These are frequencies at which the system has a natural tendency to vibrate. If the forcing frequency corresponds to one of these natural frequencies, the resulting amplitude of vibration of the structure is maximized.

We can take as an example the vibrating beam provided in Figure 3.2. Its resonance frequency is generalized according to the following formula [1]:

$$f_r = \beta(\frac{h}{L^2})\sqrt{\frac{E}{\rho}} \tag{2.1}$$

[1] The piezoelectric thickness t_{pieze} have to be equal to $\frac{\lambda}{2}$, λ is the input wavelength.

Where β is a dimensionless coefficient that is determined by the shape of the vibration mode, E is the Young's modulus and ρ is the density.

The resonance frequency of an acoustic wave resonator depends mainly on its material composition, shape and volume.

3.2.2 **Transduction**

Generally, MEMS resonators are interfaced with electronic circuits. That is why the resonator mechanical vibration should be actuated and sensed by an electrical signal. The choice of mechanism through which the electrical energy is reciprocally converted to mechanical vibration (or the inverse) plays the essential role in the overall performance of the resonator. Factors associated with the transduction mechanism such as efficiency of the energy conversion, insertion losses, implementation simplicity and power consumption should be carefully considered and analyzed. Some of the most commonly used transduction mechanism are capacitive, piezoelectric, thermal, piezoresistive…

In the particular case of acoustic resonators, transduction efficiency is quantified with the electromechanical coupling factor:

$$K_t^2 = \frac{stored\ mechanical\ energy}{provided\ electrical\ energy} = \frac{stored\ electrical\ energy}{provided\ mechanical\ energy} \tag{2.2}$$

3.2.3 **Losses and quality factor**

The quality factor, noted Q, is one of the performance criteria of resonators. It represents energy losses. The quality factor is defined as the ratio of system losses to energy stored during a cycle of vibration. We are naturally looking for resonators with quality factors as high as possible

In fact, a portion of the energy stored in a MEMS resonator (such as elastic energy for an electromechanical resonator) escapes the system in the form of acoustic or electromagnetic waves or in the form of heat within the resonator. Different mechanisms can be the cause of such losses such as viscous losses, anchor losses, material losses… If the energy loss for each mechanism is given, the overall quality factor of the resonator can be found by summing up the dissipated energies and the total quality factor will be equal to [1]:

$$Q_{total} = \left(\sum \frac{1}{Q_i}\right)^{-1} \tag{2.3}$$

Where Qi corresponds to damping from each potential loss mechanism.

3.3 Equivalent electrical circuit

In order to be able to use electromechanical resonators in electrical circuits and to facilitate their design, it is important to assign them an equivalent electrical circuit. Here I will present an electrical equivalent model of an electromechanical resonator, giving specific examples in the case of a piezoelectric resonator. To do this, we start with a mechanical model of the resonator, modelled by a mass-spring-damper system (Figure 3.3). We can then deduce the equivalent electric circuit by using electromechanical analogies (Table 3-1)

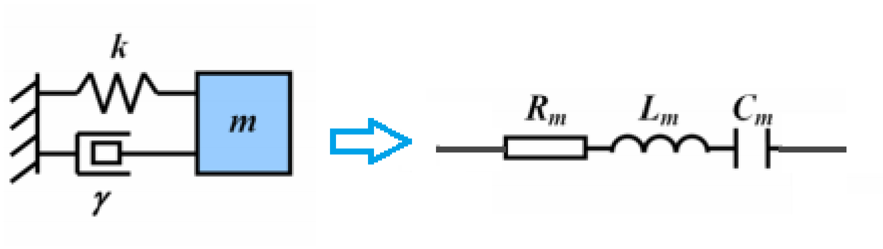

Figure 3.3 A MEMS resonator can be modeled in the mechanical domain by a mass m, stiffness k, and damping factor γ. With analogies, we get the resonator electromechanical mode, inspired from [1]

Table 3-1 : Analogy between mechanical and electrical domains

Mechanical Domain	Electrical Domain
Force, F	Voltage, V
Velocity, $\dot{x}$	Current, i
Displacement, x	Charge, q
Compliance, $1/k$	Capacitance, C
Mass, M	Inductance, L
Damping, γ	Resistance, R

This mechanical analogue of a RLC circuit is called the motional arm. It takes into account both the mechanical motion and its transduction. The capacitance, for the first harmonic of resonance, can be calculated as follows [2]:

$$C_m = \frac{\eta^2}{k} \tag{2.4}$$

The motional inductance L_m is as following:

$$L_m = \frac{M}{\eta} \tag{2.5}$$

And the motional resistance is:

$$R_m = \frac{\gamma}{\eta^2} \tag{2.6}$$

With η the coupling factor that is defined as the ratio of displaced charge and spatial displacement, which represents the transduction efficiency:

$$\eta = q/x \tag{2.7}$$

Therefore, low losses and a good transduction result in a small motional resistance. For this reason, the motional resistance is one of the main performance indicators of MEMS resonators.

In practice, signals of a purely electrical origin can be mixed with those coming from the motional arm. For example, electrodes (used for actuation and detection), together with the dielectric piezoelectric material form a capacitance called static capacitance, described as

$$C_0 = \frac{\epsilon\epsilon_r A}{t} \tag{2.8}$$

Where ϵ_r is the dielectric permittivity, A is the electrode area and t is the dielectric thickness.

To better describe the resonator response, an additional resistance is added and placed in series with the capacity C_0. This resistance R_0 models the dielectric losses in the resonator. The final electrical model of the resonator is called Modified-BVD (MBVD) (Figure 3.4). It approximates the resonator impedance close to the resonance frequency.

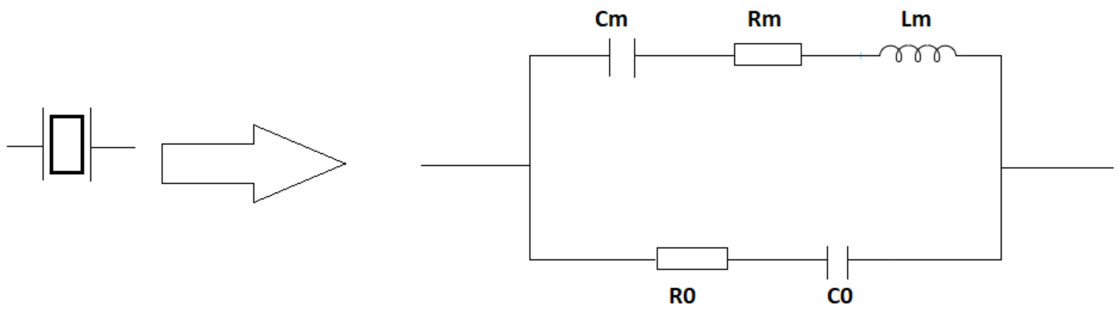

Figure 3.4 : The modified BVD model of the MEMS resonator

We can model the equivalent impedance given by the MBVD model. The formula (2.9) shows the equation relating the complex impedance to the complex admittance:

$$Z = \frac{1}{Y} \tag{2.9}$$

And let's suppose that

$$Z = R + JX \tag{2.10}$$

With R and X respectively the real and the imaginary part of the impedance, so we have that:

$$|Z| = \sqrt{R^2 + X^2} \tag{2.11}$$

$$R = |Z|\cos(\beta) \tag{2.12}$$

$$X = |Z|\sin(\beta) \tag{2.13}$$

Where β is the impedance phase. The impedance described by the MBVD model results in a resonance and anti-resonance behavior, caused by the interaction of the current along both arms of the model. The resonance and the anti-resonance of the resonator occur when the impedance becomes purely resistive, which only happens at two frequencies for a given resonance mode. At these points, the phase is equal to zero. The one with the lower frequency is the resonance frequency that represents the minimum magnitude of the impedance and the other is the anti-resonance frequency that represents the maximum magnitude of the impedance, as shown in Figure 3.5. Both of these particularities are used to get the resonance and anti-resonance frequencies, either from the maximums of $|Z|$ and $|Y|$ or from the admittance/impedance phase graphs.

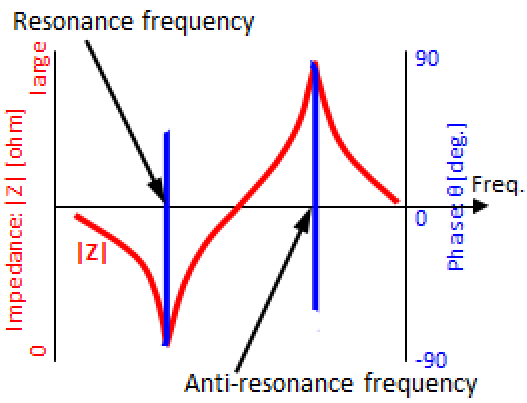

Figure 3.5 : Resonance and anti-resonance frequencies in the impedance curve of a piezoelectric resonator

From the impedance given by the MBVD model we can obtain the transfer function of the resonator [4]:

$$H = \frac{V_s}{V_e} \tag{2.14}$$

With V_s and V_e are respectively the input and the output voltages. If Z_{11} is the input impedance at the resonance frequency, the input voltage is

$$V_e = I_e * Z_{11} \tag{2.15}$$

Where I_e is the input current.

The transfer function becomes:

$$H = \frac{V_s}{V_e} = \frac{V_s}{I_e * Z_{11}} = \frac{1}{Z_{11}} * \left(\frac{-\mathrm{W}^2 * \left(\frac{\mathrm{C_m}}{\alpha} + \frac{\mathrm{C_0}}{\beta}\right) + \mathrm{j}(\mathrm{C_m} * \mathrm{W} + \mathrm{C_0} * \mathrm{W} - \mathrm{C_0 C_m L_m W^3})}{1 - \mathrm{W}^2\left(\mathrm{C_m L_m} + \frac{1}{\alpha * \beta}\right) + \mathrm{j} * \left(\frac{\mathrm{W}}{\alpha} + \frac{\mathrm{W}}{\beta} - \frac{\mathrm{C_m L_m W^3}}{\alpha}\right)} \right) \tag{2.16}$$

With :

$$\alpha = \frac{1}{R_0 C_0} \quad (2.17)$$

$$\beta = \frac{1}{R_m C_m} \quad (2.18)$$

$$W = 2\pi f \quad (2.19)$$

To better understand the electrical model parameters of the resonator, it will be useful to detail how each parameter affects the resonator's response (all the following graphs are based on the parameters of a measured resonator). C_m and L_m determine the resonator's resonance frequency (Figure 3.6).

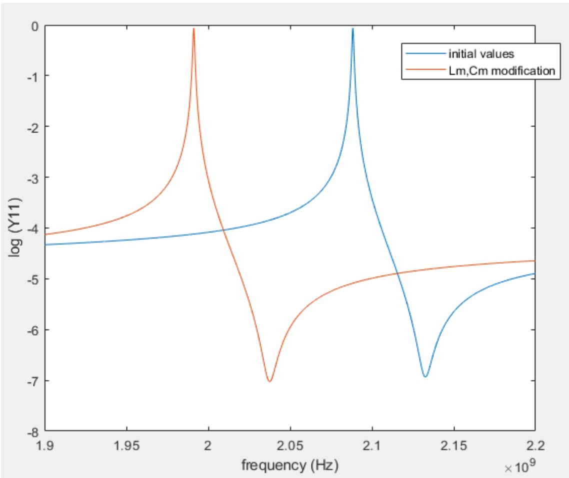

Figure 3.6 : Comparison between initial MBVD values results and the resonator response after a change in Lm or Cm.

C_0 is the electrical capacity of the resonator, which dominates at frequencies far away from resonance. As shown in Figure 3.7, C_0 mainly affects the anti-resonance frequency and amplitude.

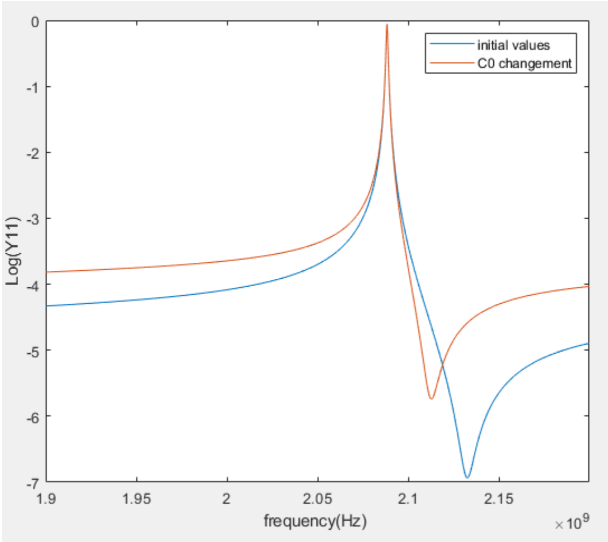

Figure 3.7 : Comparison between initial MBVD values results and the resonator response after a change in C0.

R0, the static resistance, models the impedance/admittance amplitude and quality factor at the anti-resonance frequency as shown in Figure 3.8.

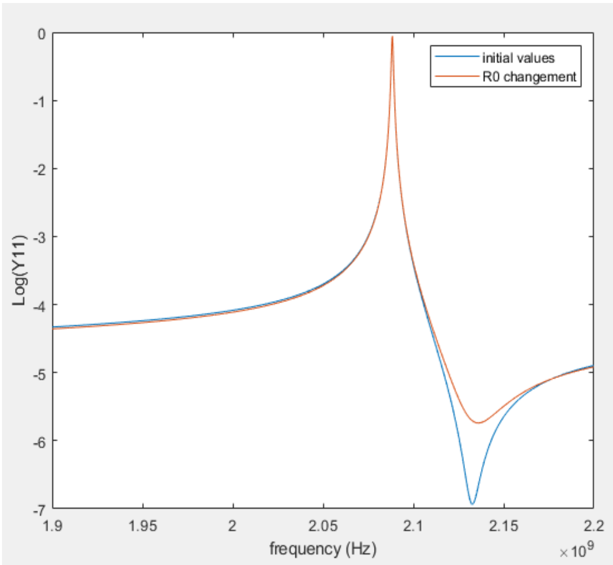

Figure 3.8 : Comparison between initial MBVD values results and the resonator response after a change in R0.

Rm, the motional resistance, affects the magnitude of the resonator's impedance/inductance and the resonator's quality factor (Figure 3.9).

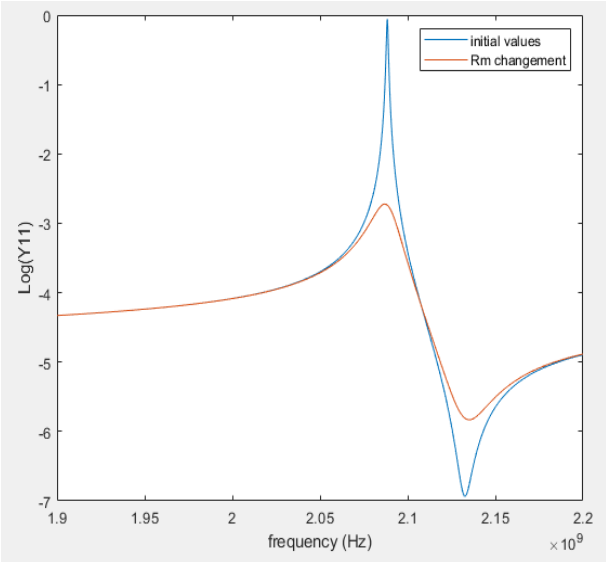

Figure 3.9 : Comparison between initial MBVD values results and the resonator response after a change in Rm.

As mentioned above, the motional resistance Rm affects the level of signal that we can extract from the resonator for a given input power. A low Rm means a larger amplification of the input power due to the resonance phenomenon.

4 Characterization of MEMS resonators

The first step in the development of MEMS resonators-based clocks is a study and a characterization of resonators available in CEA-LETI. This is primordial in order to check if they can meet 5G clocks' specifications, mainly in terms of resonance frequency and motional impedance. This chapter first presents the devices that will be studied, then the measurement instruments and protocol followed by a presentation of results and an extraction of parameters for their electrical equivalent models.

4.1 MEMS resonators at LETI

As mentioned above, CEA-LETI has a large background in the development of MEMS resonators. Among these microelectromechanical structures, BAW (Bulk Acoustic Wave) resonators represent a technology with potential to reach 5G specifications in terms of resonance frequency and quality factor.

The most simple BAWs can be conceived as a structure consisting of a piezoelectric material sandwiched between two electrodes (top and bottom), which are surrounded by vacuum (or air). When an oscillating voltage difference is applied to the electrodes, an acoustic wave that propagates in the material (Figure 4.1) is generated. The longitudinal mode is the main mode of operation of BAW resonators: the bulk acoustic wave travels from one electrode to another and reflects on the vacuum surrounding the electrodes. The resonance is caused by the constructive interference of such reflected waves, which is the case of the FBAR (Film Bulk Acoustic Resonator). This can be seen as the mechanical equivalent of a transmission line resonator, where the vacuum acts as a short circuit. Two other BAW technologies can be presented depending on the way to realize the acoustic isolation of the resonator: SMR (Solidly Mounted Resonator) and HBAR (High Overtone Bulk Acoustic Resonator). A detailed characterization of these two BAW technologies is presented below.

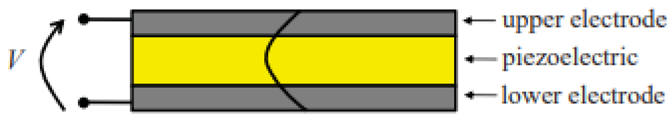

Figure 4.1 : schematic representation of a BAW resonator showing both upper and lower electrodes where a voltage is applied and the piezoelectric material that generates the acoustic wave

4.1.1 Surface mounted resonators: BAL2

The first characterization work is done with one-port BAW-SMR resonators included in layout named "BAL2". The principle of BAW-SMR is to use a Bragg reflector to insure acoustic isolation instead of an air/vacuum interface (Figure 4.2). This reflector is the transposition of a principle widely exploited in optics, which is the "mirror of Bragg". In the mechanical domain, this is accomplished by using a stack of materials with different acoustic impedances (for an analogy between the optical and mechanical domains, see Table 4-1).

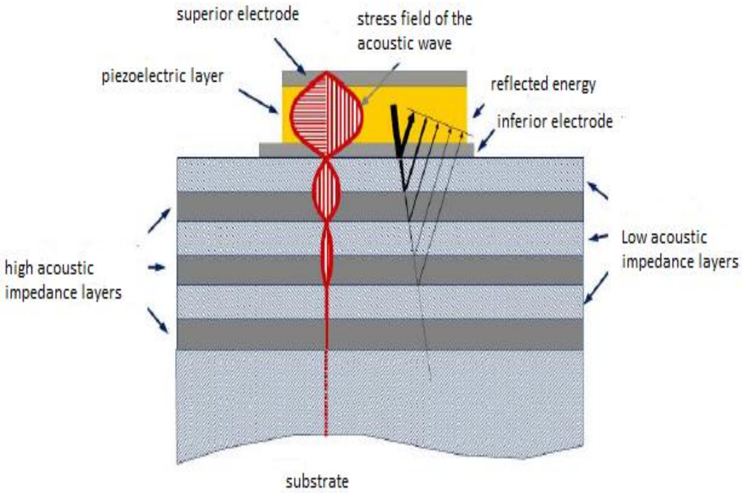

Figure 4.2 : Schematic of a BAW-SMR device showing the substrate with different impedance layers and sandwiched piezoelectric material. It shows the waves propagating in the substrate and the piezoelectric layer too, modified from [5].

Table 4-1 : Analogy between the optic domain parameters and the acoustic ones.

Optic	Acoustic
Electrical field E	Acoustic pression P
Optical index n	Acoustic slowness S= 1/V
Optical impedance 1/n	Acoustic impedance Z_a

In practice, the mirror is built by an alternating stack of quarter-wave layers (λ/4) of low and high acoustic impedance under the active part of the resonator, where λ is the acoustic wavelength in the material at the resonance frequency of the resonator. A λ/4-thickness of the Bragg layers (thickness compared with the wavelength of the acoustic wave) makes it possible to obtain reflected waves in phase with the incidental waves, ensuring maximum reflectivity. Figure 4.3 shows the BAL2 layout, with an example of one of the characterized devices

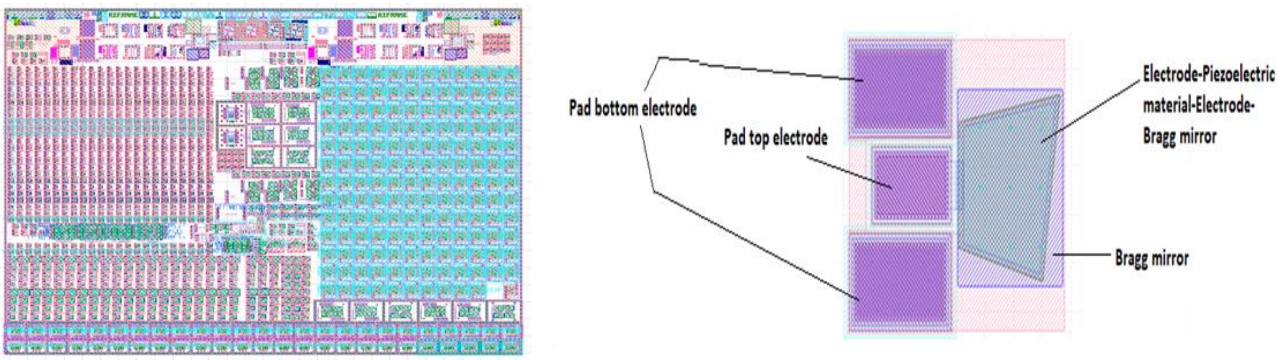

Figure 4.3 : BAL2 layout. Left: general view of the whole layout. Right: detail of the resonators under measurements with a brief description of different layers.

4.1.2 **High-Overtone Bulk Resonator : ORAGE**

The second characterization concerns HBAR resonators done in LETI in the context of the project "ORAGE". A HBAR resonator is obtained by stacking a thin piezoelectric film over a low acoustic loss substrate. The piezoelectric film, by converting an incoming exciting electrical signal, generates an acoustic wave. The piezoelectric film and the two electrodes on its both sides are used as a transducer whereas the acoustic energy is mainly confined in the substrate (Figure 4.4).

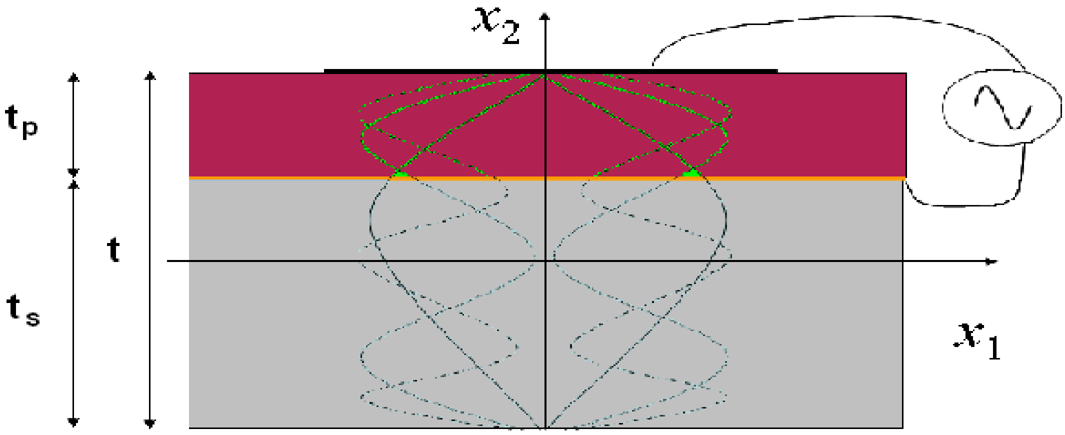

Figure 4.4 : Schematic of a HBAR resonator, tp is the piezo layer and ts is the substrate layer, [6]

The HBAR resonators under measurement consists of two 1-port HBAR resonators close enough to ensure acoustic coupling via evanescent waves (Figure 4.5): when we excite the first resonator, its vibration induces a motion in the second resonator which we measure. Double-port HBAR resonators have a great interest to simplify the development of an oscillator (see chapter5), and they are less sensitive to parasitic electrical currents than other configurations.

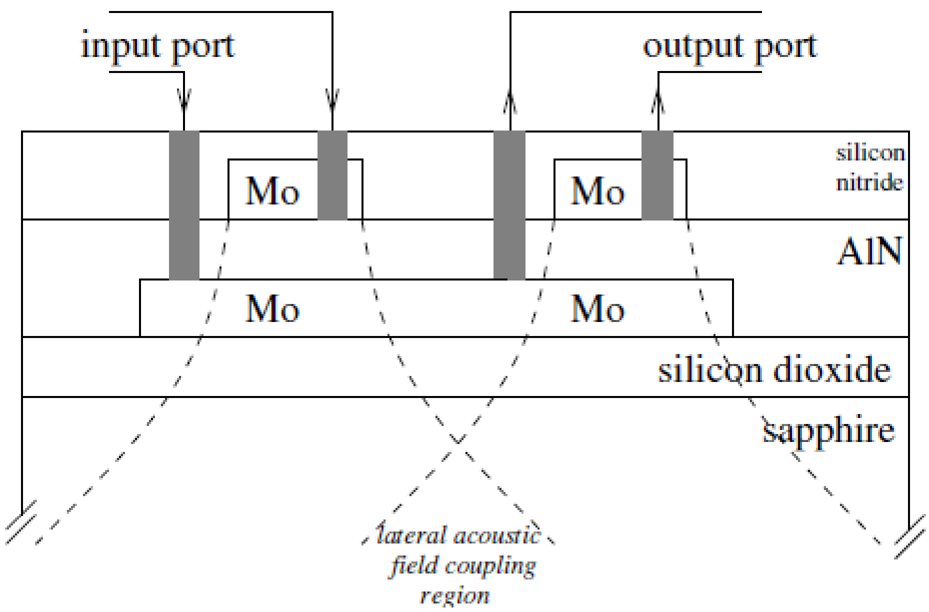

Figure 4.5 : Schematic of the cross section of a 2-port laterally coupled HBAR, modified from [31].

4.2 Measurements

The devices are measured on wafer, using electrical probes which directly contact the electrodes without need of packaging. In order to perform such measurements, I got habilitations to operate a RF probe station and a Vector Network Analyzer (VNA). The RF probe station contains the means to electrically contact the devices under test, while the VNA is the measurement instrument.

In the first part of this section I will present the instruments used in the measurements, followed by the measurement protocols. In the second part, I will present measurement results and equivalent electrical models.

4.2.1 Instruments

4.2.1.1 Probe measurements

4.2.1.1.1 Probe station: SIGNATONE CM460

The CM460 is a semi-automatic probe station, rich in features and capabilities that offer a human engineered interface to make operation easy and intuitive. It can be used for a variety of probing applications such as microwave probing, low current probing, thermal probing… The probe station is used, in our case, for positioning RF probes on electrical contact pads on a wafer, so that our devices can be tested. It consists of a plate called "chuck" to hold the wafer and a "stage" to precisely position the device under the probes. The user installs probe arms and tips in the immobile body of the station, called the "platen" and uses a microscope mounted above the platen to place the probe tips on the device. Figure 4.6 show the probe station we are using.

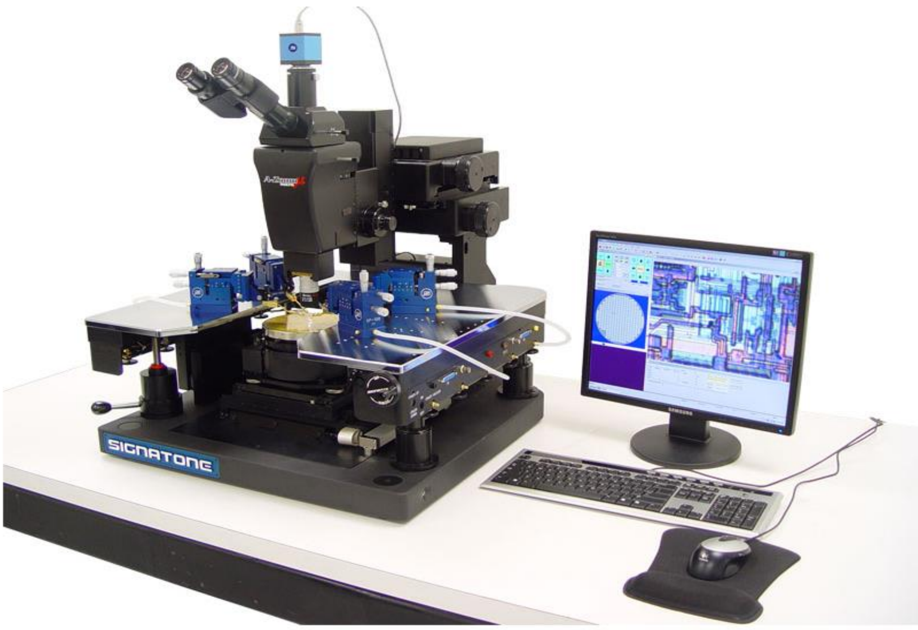

Figure 4.6: SIGNATONE CM460 probe station.

4.2.1.1.2 RF Probes: Z probes GSG (Ground-Signal-Ground)

RF probes are used to measure RF signals in electronic circuits. The probes used in our measurements are GSG (Ground-Signal-Ground) RF probes provided from Cascade Microtech with a maximum working frequency equal to 40 GHz and a 100 μm pitches (Figure 4.7).

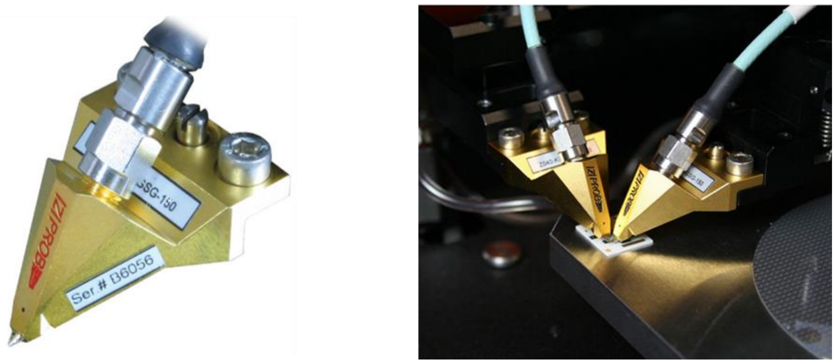

Figure 4.7 : Z probes GSG.

4.2.1.2 VNA: AGILENT N5230A

A vector network analyzer measures the module and the phase of the S-parameters of an electrical circuit. It is generally used in the RF domain in order to characterize filters, cables, antennas or, resonators, among others. The instrument that we are using is a 4-ports VNA that can work up to 20 GHz, provided by Agilent Technologies (Figure 4.8). It provides the characterization results in the form of .sXp files (X is the number of ports used in the measurements). From such files, we can extract the impedance, admittance and phase information of the device, to be post-processed later.

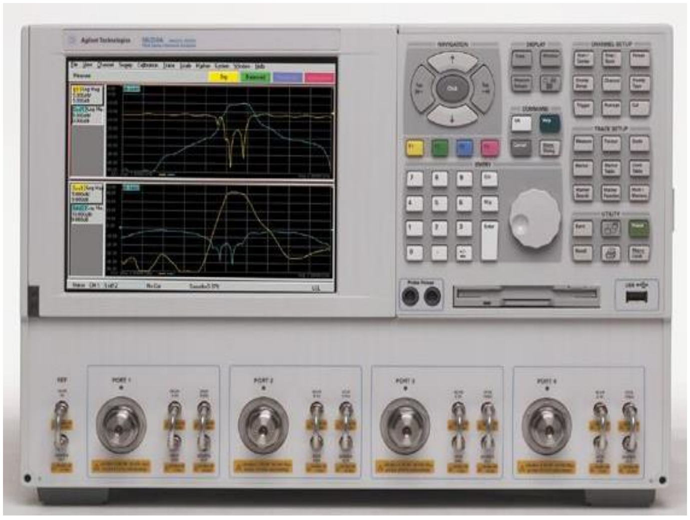

Figure 4.8 : 4-Port VNA AGILENT N5230A.

4.2.2 **Measurements protocol**

4.2.2.1 Measurements: S-parameters

Scattering parameters are the electrical characteristics of a signal in a complex network and are mostly used in RF network and applications. The VNA is the appropriate device to measure S-parameters. To clarify the S-parameters measurement principle of the VNA, let us consider the quadrupole in Figure 4.9. The scattering parameters provide information about the reflected and transmitted signals between each of the ports, information that can then be used to model the device under test.

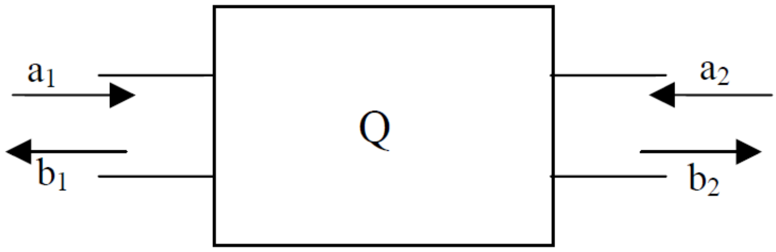

Figure 4.9 : Quadrupole, a and b are incident and reflected waves.

$$S_{11} = \frac{reflected\ wave\ in\ port1}{incident\ wave\ in\ port\ 1} = \frac{b_1}{a_1}\ |a_2 = 0$$ Reflection coefficient in port 1

$$S_{21} = \frac{transmitted\ wave\ in\ port\ 2}{incident\ wave\ in\ port1} = \frac{b_2}{a_1}\ |a_2 = 0$$ Transmission coefficient port1-port2

$$S_{12} = \frac{transmitted\ wave\ in\ port\ 1}{incident\ wave\ in\ port\ 2} = \frac{b_1}{a_2}\ |a_1 = 0$$ Transmission coefficient port2-port1

$$S_{11} = \frac{reflected\ wave\ in\ port\ 2}{incident\ wave\ in\ port\ 2} = \frac{b_2}{a_2}\ |a_2 = 0$$ Reflection coefficient in port 2

4.2.2.2 VNA Calibration

The Network Analyzer is only calibrated at its connectors for its power output, and to make dipole's or quadrupole's measurements we need to add RF cables and if necessary adapters between coaxial connectors. All these elements add losses, phase shifts and impedance mismatches, so it is required to perform a calibration process to compensate these effects. To sum up, calibration serves to determine the matrix of systematic errors of the measurement system (analyzer, cables, adapters and probes). The calibration process is performed in the same frequency range as the measurements of the device under test.

4.2.2.2.1 For 1-port measurements

One-port measurements are based on the S_{11} parameter, so we need to consider three main errors: directivity, mismatching and frequency response detector. These errors will generate three error coefficients E1, E2, E3 (the vector of systematic errors) in the equation relating real S_{11} (S_{11r}) to the measured one (S_{11m}). Let's suppose $S_{11r} = F(S_{11m})$, in order to get S_{11r}, we need to know F so we need to know E1,E2 and E3 (they are F parameters). At this step, we have three independent unknowns, so we need three independent equations. To do that, we will make three different measurements to obtain S_{11m} (short, open and load), because we have defined the calibration substrate (csr8 in our case), and therefore we know the expected S_{11r}. With this procedure, the VNA can solve the system and obtain the calibration function.

4.2.2.2.2 For 2-port measurements

The calibration principle for 2-port measurements is the same as for the 1-port, but we have more unknowns. Therefore, we need to calibrate each individual port as explained in before (short, open and load for each), and additionally perform a thru calibration. The thru is used to describe the main transmission state between the two ports in the calibration substrate and calibrate it to get, after calibration, an S matrix equal to:

$$S = \begin{pmatrix} 0 & 1 \\ 1 & 0 \end{pmatrix} \tag{3.1}$$

The following figure (Figure 4.10) shows an example of a VNA 2-port calibration, for frequencies between 500 MHz and 5GHz.When we measure a load, we distinguish that S11=S22 and S12=S21=1. That means that after calibration, we have an exact point on the 50Ω load on the smith chart (there are no mismatches). Adding to that, the power is transmitted completely from port 1 to port 2 and vice versa.

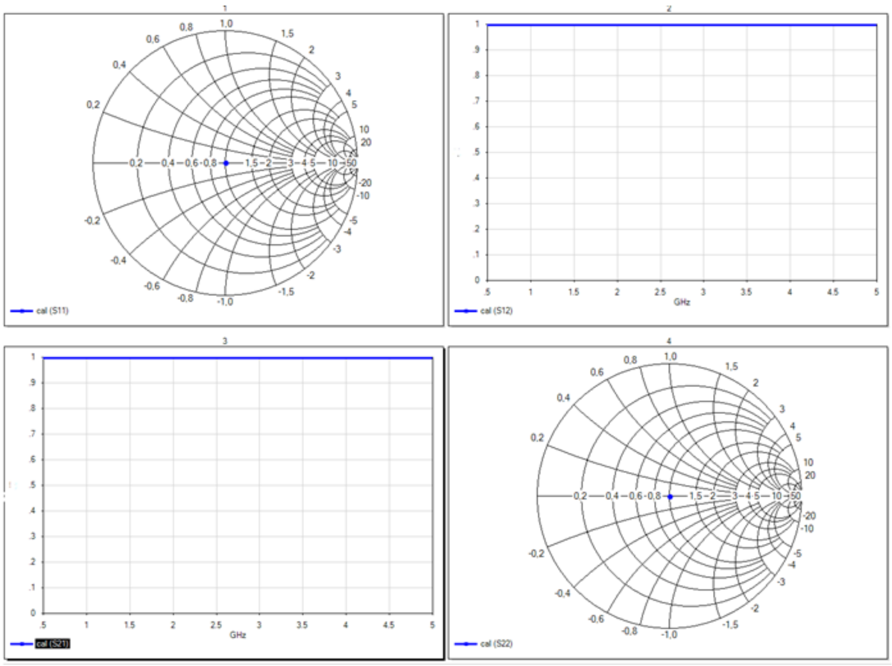

Figure 4.10 : Example of a 2-port calibration Load result containing S11, S22, S12 and S21 plots.

4.3 Measurement results, parameter extraction and fitting

As mentioned above, to get the complete knowledge about the resonator performances and for further uses, we need to make .sXp files, provided by the VNA, understandable, clear and exploitable. The first step in this process is to develop a MATLAB code to treat the .sXp files. This code can be found in the appendix [A] and it shows how we can get admittance, impedance, S and phase graphs in a precise frequency segment of the measured frequency range. The code adjusts the measured data to the equivalent MBVD model of the DUT and provides relevant parameters such as the quality factor and the electromechanical coupling coefficient K_t^2.

4.3.1 Resonator performances

4.3.1.1 Solidly mounted resonators (BAL2)

I measured different resonators present in the BAL2 chips. Figure 4.11 shows a superposition of some of these measurements. We see that the resonance frequency of these devices is between 2 GHz and 2.2 GHz and they have approximately the same Y11 level. Different thicknesses of the piezoelectric layer of the resonators (fabrication is not being completely uniform in the wafer) can explain the peaks shifts. To get more details about the performance of this technology we will focus on the study of one of them, E5H17.

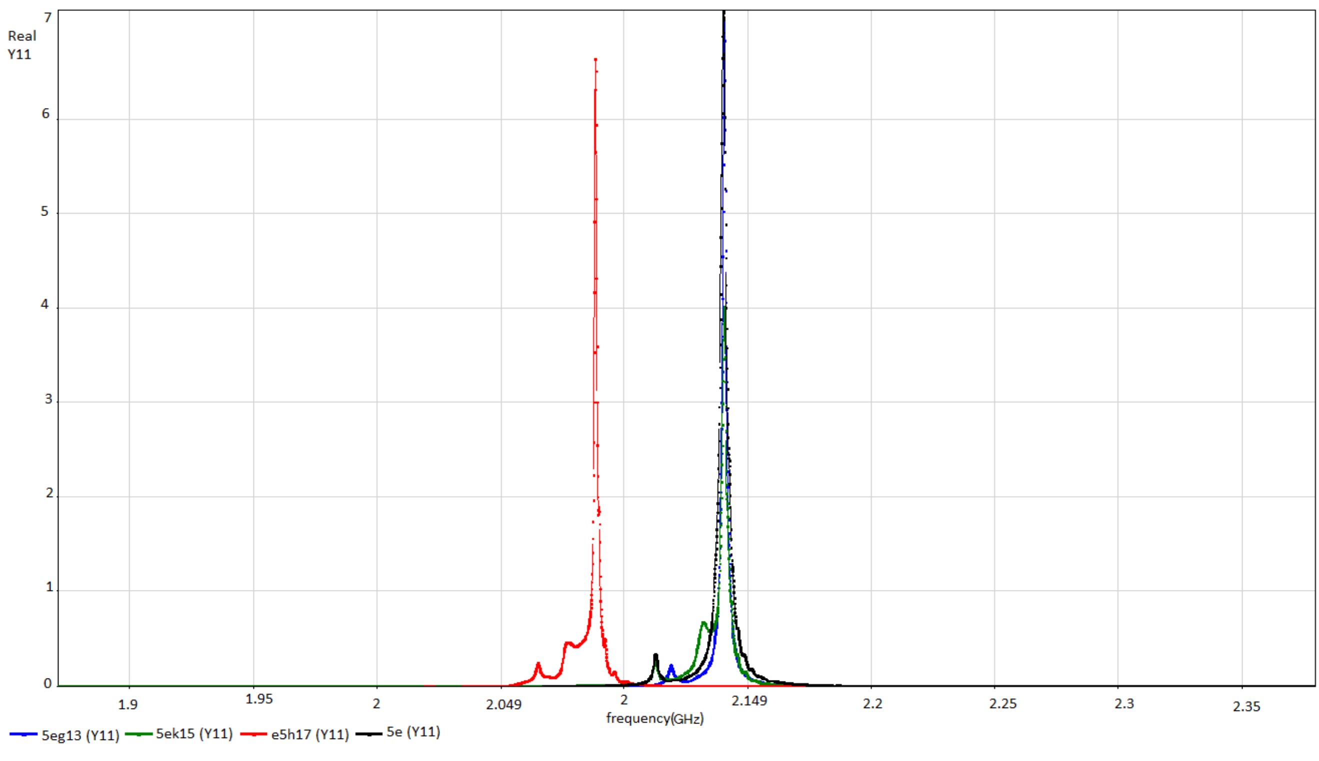

Figure 4.11 : Superposition of different measurement results: Y11(S) magnitude VS frequency (GHz).

The chosen resonator, as can be seen in the Figure 4.12, has a resonance frequency equal to 2.0884 GHz and anti-resonance frequency equal to 2.1310GHz. The quality factor of the resonance frequency is 1900 and the electromechanical coupling coefficient K_t^2 is equal to 4.84%. These values are calculated from the following formulas [9], [3]:

$$k_t^2 = \frac{\left(\frac{\pi}{2}\right)^2 (f_p - f_s)}{f_p} \tag{3.2}$$

$$Q = \frac{w_s L_m}{R_m} \tag{3.3}$$

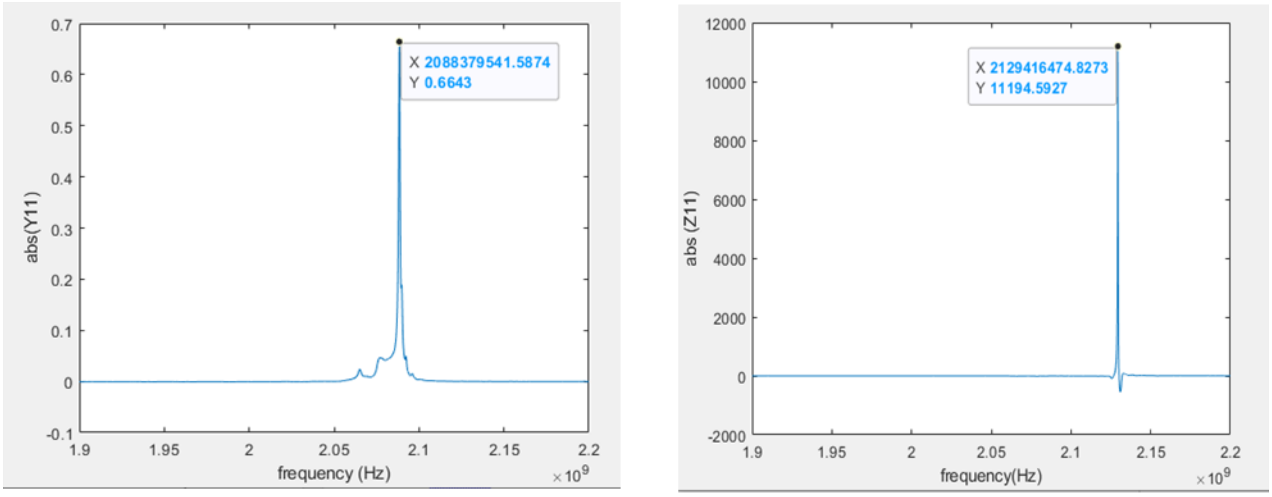

Figure 4.12 : E5H17 measurement results. The left side of the plot is the Y11(S) magnitude vs frequency. The maximum admittance corresponds to the resonance frequency. The right side is the Z11(Ω) magnitude vs frequency. The maximum of resistance corresponds to the anti-resonance frequency.

4.3.1.2 High-overtone bulk resonators (ORAGE)

As it was done with BAL2 devices, I measured different 2-port resonators present in the ORAGE mask. All the resonators' responses have approximately the same shape: an envelope signal comprising different modes of resonance due to the piezoelectric (AlN) mechanical properties (for example, the peaks at 3.8 GHz and 4.3 GHz of Figure 3.13). In addition, inside this envelope we distinguish different oscillations caused by confined waves in the sapphire substrate that are, after that, reflected at its interface on the back of the wafer. To properly study these resonators, we will focus on the E3B4 resonator present in the ORAGE mask.

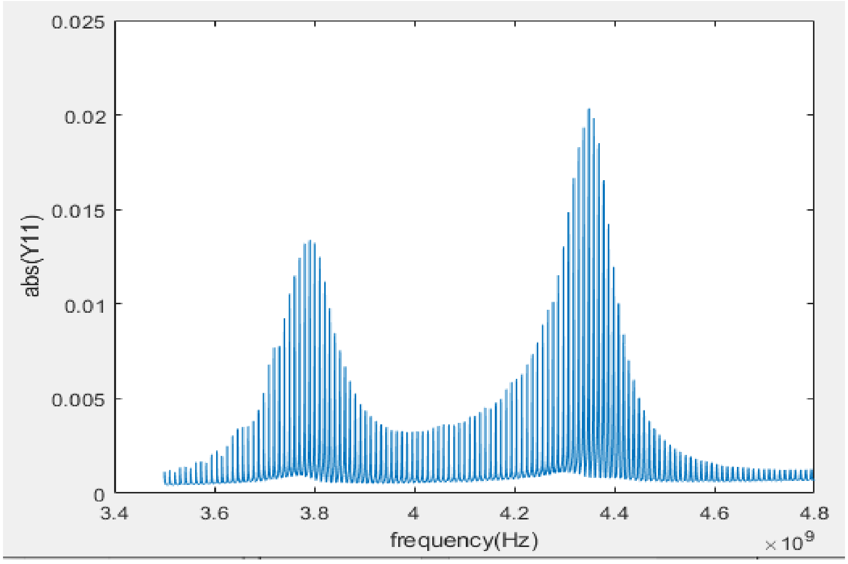

Figure 4.13 : Admittance of 2-port HBAR resonators response: abs (Y11)(S) vs frequency.

The admittance measurements of Figure 4.13 show different resonances equispaced with $\Delta f = \frac{c}{2t} = 10MHz$ (t is the substrate thickness). This fact is consistent with their origin being in the waves reflected by the back of the wafer, as explained above. We choose the resonance mode with the highest admittance (Figure 4.14), which will be studied in detail.

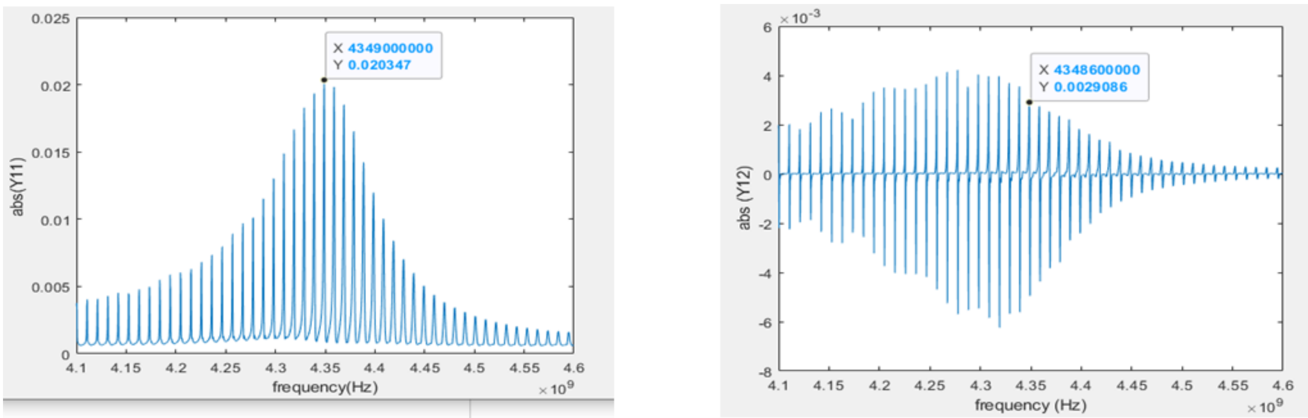

Figure 4.14 : E3B4 measurement results. Left: abs(Y11)(S) vs frequency. Right: abs(Y12)(S) vs frequency.

The resonance frequency for the E3B4 resonator is equal to 4.3488 GHz and the quality factor at resonance frequency is equivalent to 6700. A detailed view of the resonance is shown in Figure 4.15.

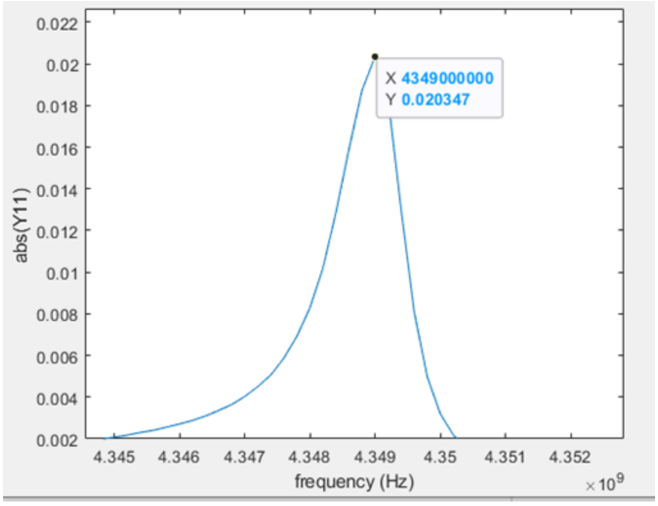

Figure 4.15 zoom on the E3B4 behavior around its resonance frequency.

4.3.2 **Parameter extraction and fitting**

This subsection is a prelude to the exploitation of the resonators shown before as time references. I developed a MATLAB code in order to get the parameters of the equivalent MBVD electrical model of the resonators, and to fit its result to the measurement results aiming to get superposed graphs. The code is included in appendix [B].

4.3.2.1 Solidly mounted resonator (BAL2)

The Table 4-2 shows the parameters extracted from the measurement of the E5H17 resonator, and the Figure 4.16 shows a comparison between measurement results and the fitted MBVD model.

Table 4-2 : Parameters extraction for E5H17 resonator

C_m	$0.3775e^{-13}F$
L_m	$15.382e^{-8}H$
R_m	1.062Ω
C_0	$0.8862e^{-12}F$
R_0	5.88Ω

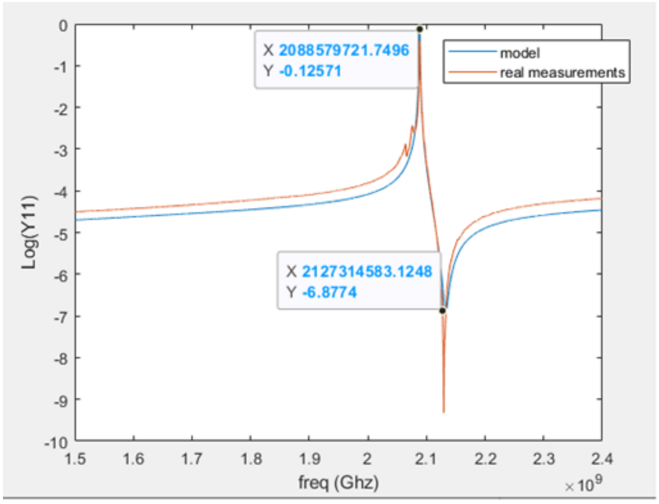

Figure 4.16 : comparison between the electrical model results and the real resonator results: log (Y11) VS frequency

4.3.2.2 High-overtone bulk resonators (ORAGE)

The MBVD model only considers a single resonance, and it is therefore not capable to describe the envelope present in the response of the ORAGE resonators. It is however a good tool to describe its behavior around a single resonance frequency. The Table 4-3 shows the parameters extracted from the measurements of E3B4 resonator and the Figure 4.17 shows a comparison between measurement results and the extracted MBVD model.

Table 4-3 : Parameters extraction for E5H17 resonator.

C_m	$1.5784e^{-16}F$
L_m	$8.48487e^{-6}H$
R_m	45.4795Ω
C_0	$4.136e^{-13}F$
R_0	0.032215Ω

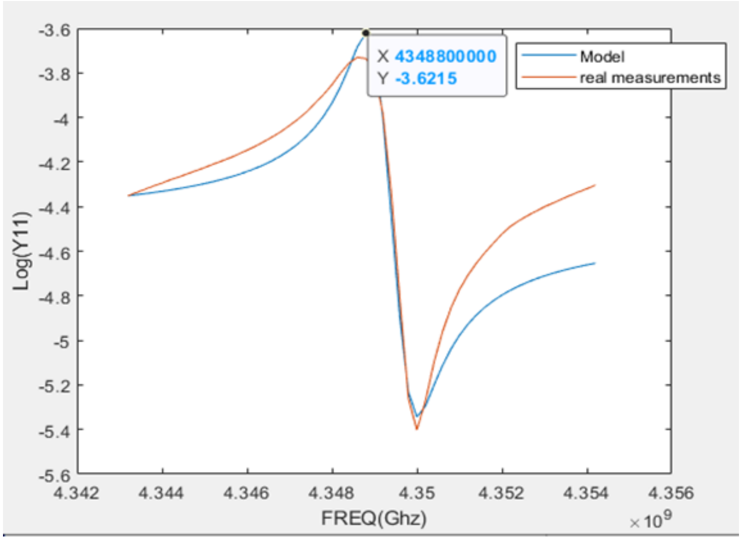

Figure 4.17: comparison between the electrical model results and the real resonator results : log (Y11) VS frequency.

5 MEMS for timing applications

In this chapter, we will introduce the application of MEMS resonators in the field of time references, and their most important parameters. These are the resonance frequency, which sets the output frequency of the time reference, and performance of the device, set by its precision and stability (translated to jitter and phase noise).

5.1 MEMS as frequency-setting elements

Growth and demand for wireless products which are at the same time portable, lightweight, consume less power and are easy to handle has boosted research on a fully integrated transceivers. MEMS clocks provide a promising solution for applications where size and degree of integration are crucial. The frequency selector for MEMS clocks is the MEMS resonator. Its performance is mainly determined by their quality factors Q and transduction efficiency, and therefore their motional resistance. As presented in the previous chapter, characterized MEMS resonators has shown great performance with measured quality factors and can operate in GHz frequency range.

In order to obtain a time reference from a MEMS resonator, we insert it in a self-oscillating feedback circuit (oscillator). This way the output of the circuit provides a sinusoidal wave at the resonator's resonance frequency without any external source.

5.2 Performance of MEMS clocks

The performance of a time source can be quantified by its jitter, of the deviation from a true periodic (ideal) signal ($\delta f/f_0$), for a given measurement time. For example, a jitter 10^{-6} at one second represents a deviation of 10^{-6} in the time reference each second, which is equivalent to 1 Hz for a 1 MHz time reference. Another performance indicator is phase noise, which represents the same uncertainty in the frequency domain. The interest of studying these phenomena comes from the fact that clocks signals needs to be precise and have uniform periods. This section provides some definitions of phase noise and jitter and the analytic calculations to pass from one to another.

5.2.1 Jitter

Jitter and phase noise are different ways of giving a quantification to the same phenomenon. This phenomenon is clearly seen from the jitter corner. The Figure 5.1 summarizes this phenomenon and explains the jitter. In fact, jitter is a measurement of the variations in the time domain, and mainly describes how far the signal period has moved from its ideal value.

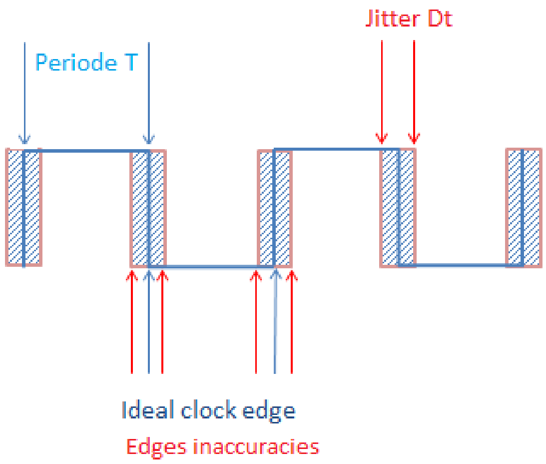

Figure 5.1 : Instability in a time signal. Dt/T is the jitter and T the square wave period.

5.2.2 **Phase noise**

In order to understand the phase noise, let S(t) a sinusoidal signal oscillating at a frequency F_0. In perfect conditions (absence of noise) the power spectral density of S will be a Dirac function at F_0. However, in practice, S(t) is accompanied with noise, which can be modelled as signals having a defined mean amplitude at different oscillating frequencies. The power spectral density of the signal plus noise is presented in the Figure 5.2 below. The noise signals are presented, in the frequency domain, as Diracs at their oscillating frequencies with amplitudes equal to the power of each signal normalized by the main signal S(t) power. In practice, phase noise produces an uncertainty in the frequency of the signal S(t), resulting in a "widening" of its spectrum.

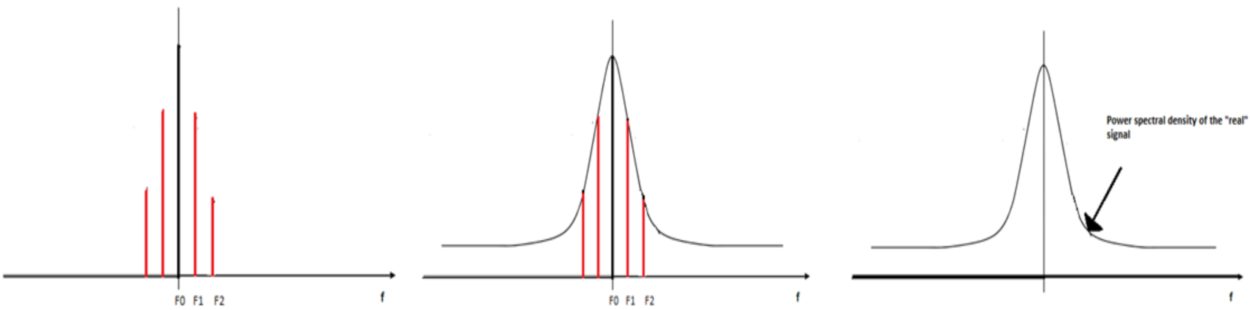

Figure 5.2 : Main signal and noise signal presentation in the frequency domain, plus detailed steps to describe how to get the power spectral density of the « real » signal.

The blue area showed in Figure 5.3 is called the right side-band. What is called the single side-band noise power density is the area beyond the signal frequency that can be considered as phase noise Figure 5.3.

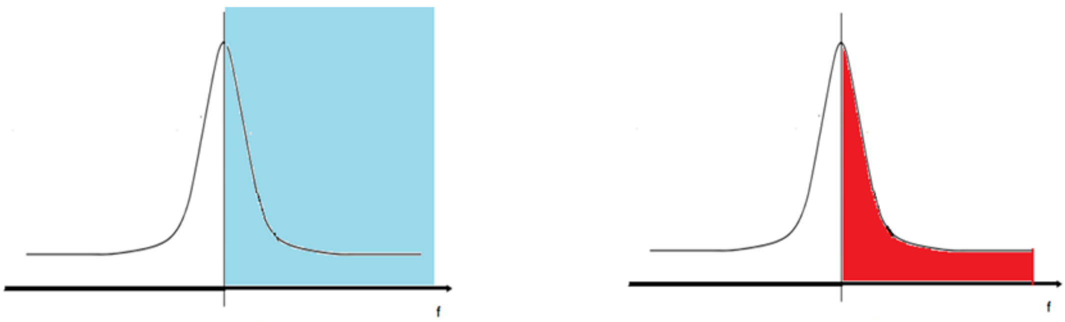

Figure 5.3 : the left plot shows the right side band. The right plot shows the total phase noise of a signal

Generally, the phase noise is defined at a specified frequency offset from the carrier F_m as the area delimited by 1-Hz bandwidth around F_m and the power spectral density curve (Figure 5.4). So, the phase noise is basically the ratio of the noise power in a 1-Hz bandwidth at a specified offset from the carrier to the carrier signal power, given in dBc/Hz.

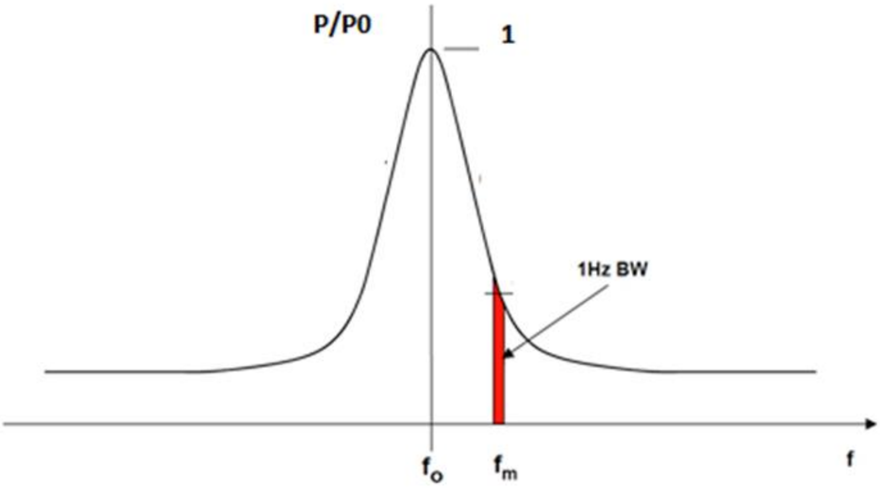

Figure 5.4 : phase noise at an offset frequency.

Apart from the resonance frequency, the quality factor of the resonator is one of the main contributors to the performance of MEMS resonators-based oscillators. Let's take the following equation which is the Leeson's equation that describes oscillator's phase noise spectrum [10]:

$$L(f_m) = 10log\left[\frac{1}{2}\left(\left(\frac{f_0}{2Q_l f_m}\right)^2 + 1\right)\left(\frac{f_c}{f_m} + 1\right)\left(\frac{FKT}{P_s}\right)\right] \quad (4.1)$$

Where f_0 is the output frequency, Q_l is the loaded Q[2], f_m is the offset from the output frequency, f_c is the 1/f corner frequency, F is the noise factor of the amplifier, K is the Boltzmann's constant, T is the absolute temperature and P_s is the available power at the sustaining amplifier input. The typical noise curve of a time reference is obtained from the Leeson's equation. It is approximated by a number of regions, each one having a slope of $\left(\frac{1}{f}\right)^k$ where k=0 corresponds to the "white" phase noise region. Regions where k=1,2,3,4 occur progressively closer to the carrier frequency (Figure 5.5). Each region corresponds to a noise type that corresponds to different origins (Table 5-1).

[2] when a resonant circuit is connected to the outside world, its total losses are combined with the load resistance. The total quality factor of this circuit is called the loaded quality factor.

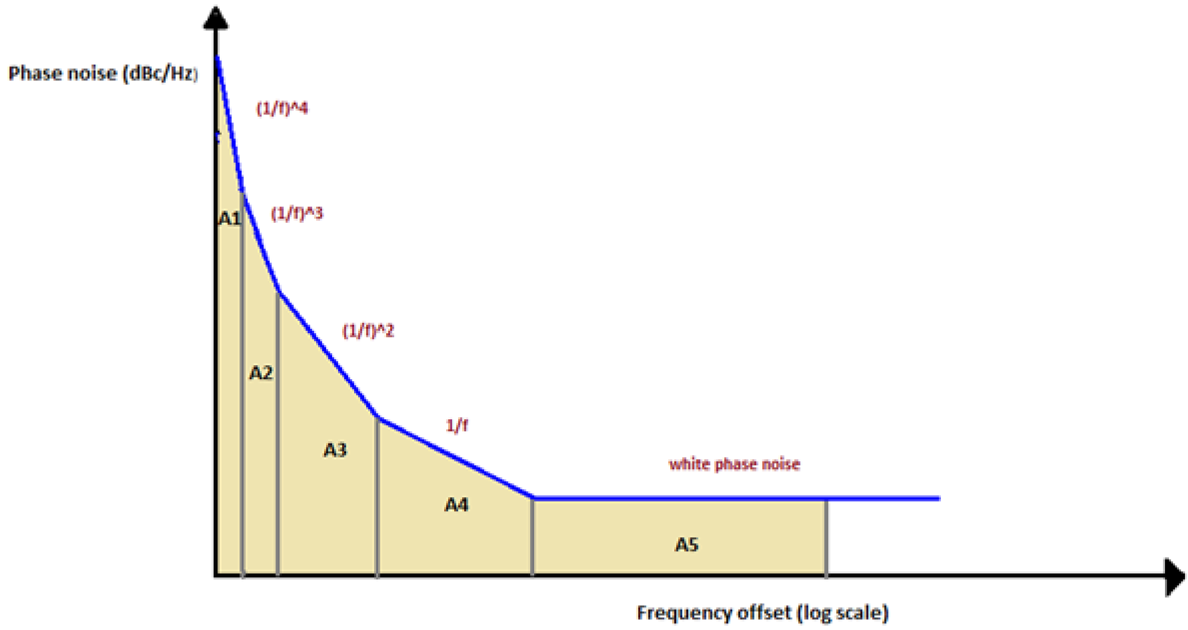

Figure 5.5 the blue curve shows an example of the phase noise profile and yellow areas are used for jitter calculation, inspired from [10], [11].

Table 5-1 : Different types of noise and its origins, inspired from [10], [11],

Slope	Noise type	Origin
f^{-4}	Random walk FM	Environment
f^{-3}	Flicker FM	Resonator
f^{-2}	White FM	Thermal noise
f^{-1}	Flicker FM	Electronic noise
1	White PM	External white noise

Near the carrier frequency, the loaded Q becomes equivalent to the unloaded Q which is the quality factor of the MEMS resonator and we have that $f_0 \approx f_m$ so to decrease the phase noise near the carrier frequency we have to increase the resonator's quality factor.

It is important to note that the main noise contributor, the term FKT/P_s, is equal to the inverse of the signal to noise ratio at the output of the amplifier, where the main noise contribution comes from the amplifier. Therefore, the maximization of signal power at the input of the amplifier, as well as the amplifier's noise, are two of the main parameters to take into consideration to optimize the performance of the time source, especially at frequencies far away from the carrier.

5.2.3 Conversion phase noise to jitter

To understand how we convert phase noise to jitter, we will start by dividing the phase noise curve into different individual areas A1, A2, A3, A4, A5 (Figure 5.5).

We call A the integrated phase noise power (dBc) and we have :

$$A = 10\log_{10}(A1 + A2 + A3 + A4 + A5) \tag{4.2}$$

We can directly calculate the RMS Jitter in seconds with the following formula *[11]*:

$$RMS\ jitter = \frac{\sqrt{2*10^{\frac{A}{10}}}}{2\pi f_0} \tag{4.3}$$

With f_0 the signal frequency.

5.2.4 **Phase noise measurements**

Phase noise measurement techniques have evolved over time along with advances in analyzer technology. As part of this internship, I used a Signal Source Analyzer to learn how to perform phase noise measurements. More specifically, the measurements were performed with a ROHDE&SCHWARZ FSUP26, which combines a phase noise tester and a spectrum analyzer (Figure 5.6). It has a frequency range from 10 MHz to 26.5 GHz.

Figure 5.6 : Signal Source Analyzer FSUP26.

I developed a Python code (APPENDIX [C]) in order to control the FSUP and to extract the resulting data that are, further, treated with Excel.

The FSUP is firstly used as a spectrum analyzer (Figure 5.7) to verify that insertion losses do not prevent the signal to pass from the port 1 to the port 2 of a 2-port resonator present in ORAGE mask. This measurement (Figure 5.7) shows a peak centered at 4.233 GHz with a power level equal to -5.61 dBm and shows white noise that is produced by the instrument.

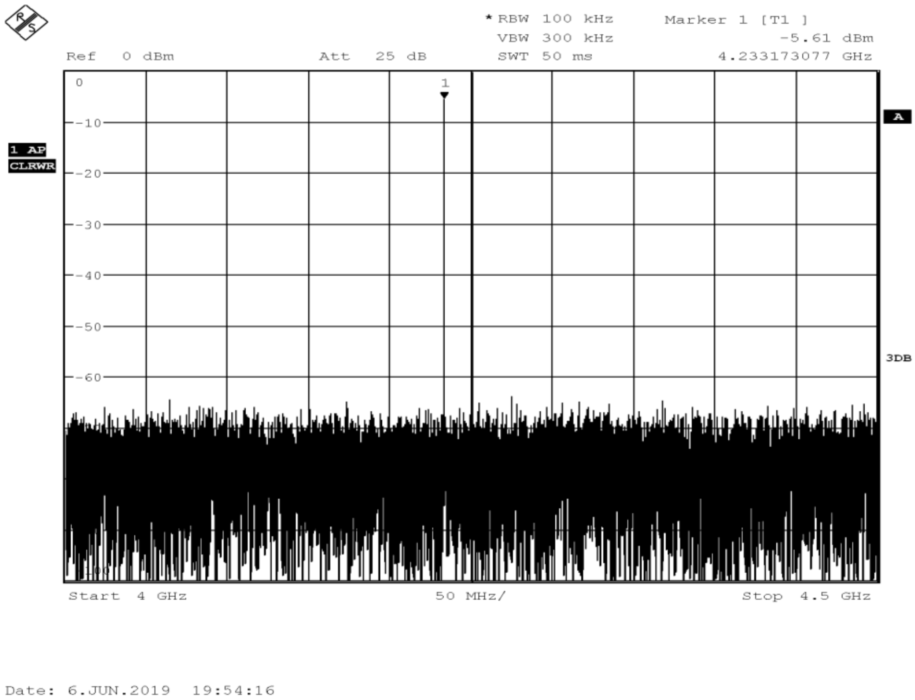

Figure 5.7: Power spectral density of a HBAR resonator.

Secondly, the FSUP is used for phase noise measurements. First, we have to declare the resonance frequency of the device under test, that is considered further as the frequency reference from which the phase noise is measured, and its power level. As we do not have MEMS oscillators available, we test the phase noise analyzer by measuring the phase noise of a RF signal source. The results are shown in Figure 5.8, and they fit with the phase noise characteristics provided by the manufacturer.

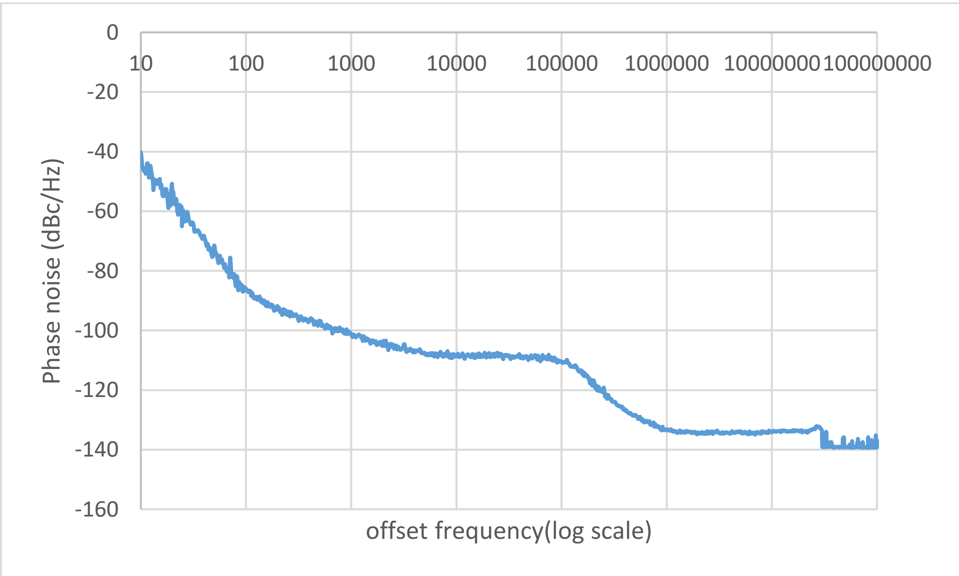

Figure 5.8 : Phase noise graph of an RF generator N5181B.

6 Resonators in closed loop

The study presented in this chapter originates from the need, presented in the previous chapter, to study the resonator in closed loop and to develop a first model of oscillator, that could later on be further improved to be a time reference. To briefly summarize the working of an oscillator, the MEMS resonator acts as the frequency selective component of an oscillator: it generates a signal from a slight stimulus at its input, and the resulting oscillations are amplified and maintained by an active element, which is, in our case, an RF amplifier. So in this chapter we deal with that configuration and with the oscillator's design steps.

6.1 Closed loop configuration

The starting point of the closed loop configuration is to use the 2-port HBAR resonator E3B4 for two reasons: firstly because of its high quality factor and resonance frequency; and secondly in order to avoid one-port resonators, since they require some transition circuits that add additional noise. The next point is to focus on the closed loop parts: the simplest oscillator consists of two essential parts, an amplifier (or gain circuit) and a resonator (Figure 6.1).

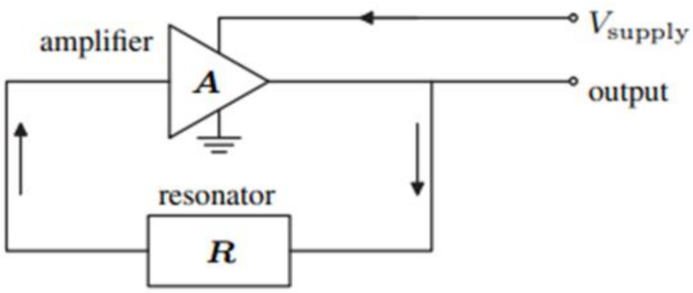

Figure 6.1 : Basic oscillator circuit [12].

The following equations represent the oscillation conditions of a closed loop configuration *[13*]:

$$Barkhaussen\ conditions : \begin{cases} \prod_{i=1}^{n} |G_i| = 1 \\ \sum_{i=1}^{n} \arg(G_i) = 0 \end{cases} \tag{5.1}$$

G_i is the transfer function of the component i and n is the number of the closed loop components. From the previously developed resonator's electrical model (Figure 6.1), we will be able to extract the transfer function of the resonator under study. In fact, it will have the following form:

$$G_{resonator} = A + iB \tag{5.2}$$

A and B are respectively real and imaginary parts of the transfer function.

At this point, we could easily say, and with referring to Barkhaussen first condition of (5.1), that the amplifier gain will be equal to the inverse of the resonator gain and its argument is equal to 0. Subsequently, with only this approach, we can not fulfill the second condition of (5.1) so we need a phase shifter to be added to the loop. This component has to satisfy two conditions: a gain equal to one and an argument equal to the opposite of the resonator's phase shift (considering that the amplifier originates no dephasing). The phase shifter will be in this case a transmission line with a length and a characteristic impedance defined below (Figure 6.2).

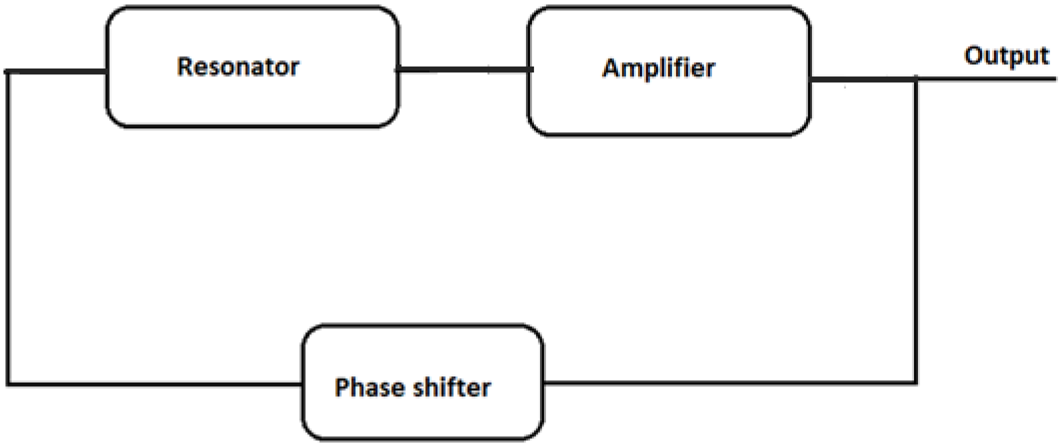

Figure 6.2 : Basic oscillator circuit taking into account Barkhaussen conditions.

Another point that needs to be highlighted is that we have to avoid impedance mismatching so we will use $\frac{\lambda}{4}$ transmission lines with:

$$\lambda = \frac{c}{\sqrt{\epsilon_r}} * \frac{1}{f_r} \tag{5.3}$$

Where c is the light velocity, f_r is the resonance frequency of the resonator and ϵ_r the relative permittivity of the material used. The characteristic impedance Z_c of a $\frac{\lambda}{4}$ transmission line is [14]:

$$Z_c = \sqrt{Z_i * Z_o} \tag{5.4}$$

Where $Z_i$and Z are respectively its input and output impedance. In addition, it keeps the signal phase constant.

To conclude, at the resonance frequency, let us suppose that z_{22} the output impedance of the resonator and 50Ω is the input and output impedance of the amplifier, to match between these two components we need to have a $\frac{\lambda}{4}$ transmission line L1. For the same reasons, the use of two $\frac{\lambda}{4}$ transmission lines L2 and L3 to match respectively the phase shifter to the resonator and the amplifier to the phase shifter. The final closed loop design is presented in Figure 6.3.

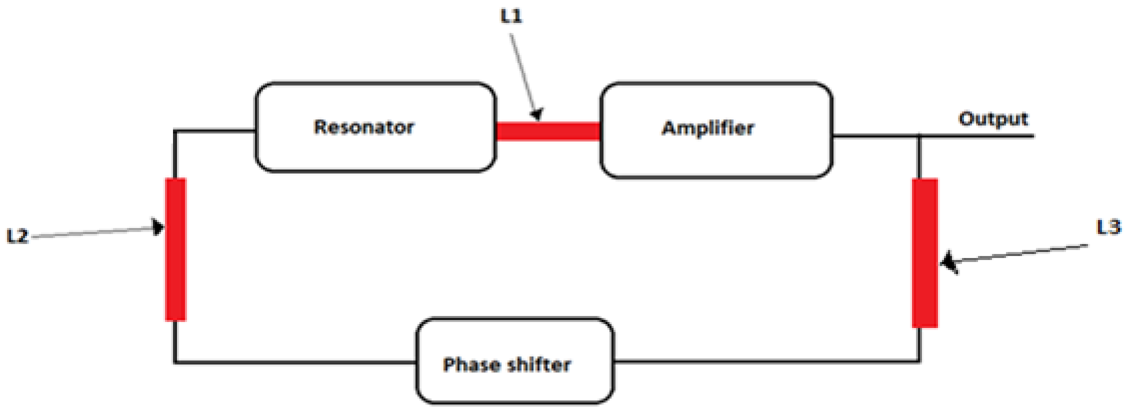

Figure 6.3 : Final closed loop configuration.

6.2 Design of the oscillator

After defining the components of the oscillator, we have to define the characteristic parameters of each component. This design is made for the E3B4 resonator.

6.2.1 Resonator

The insertion losses determine the resonator's gain that the amplifier need to compensate. S12 curve (Figure 6.4) determine the insertion losses at different frequencies.

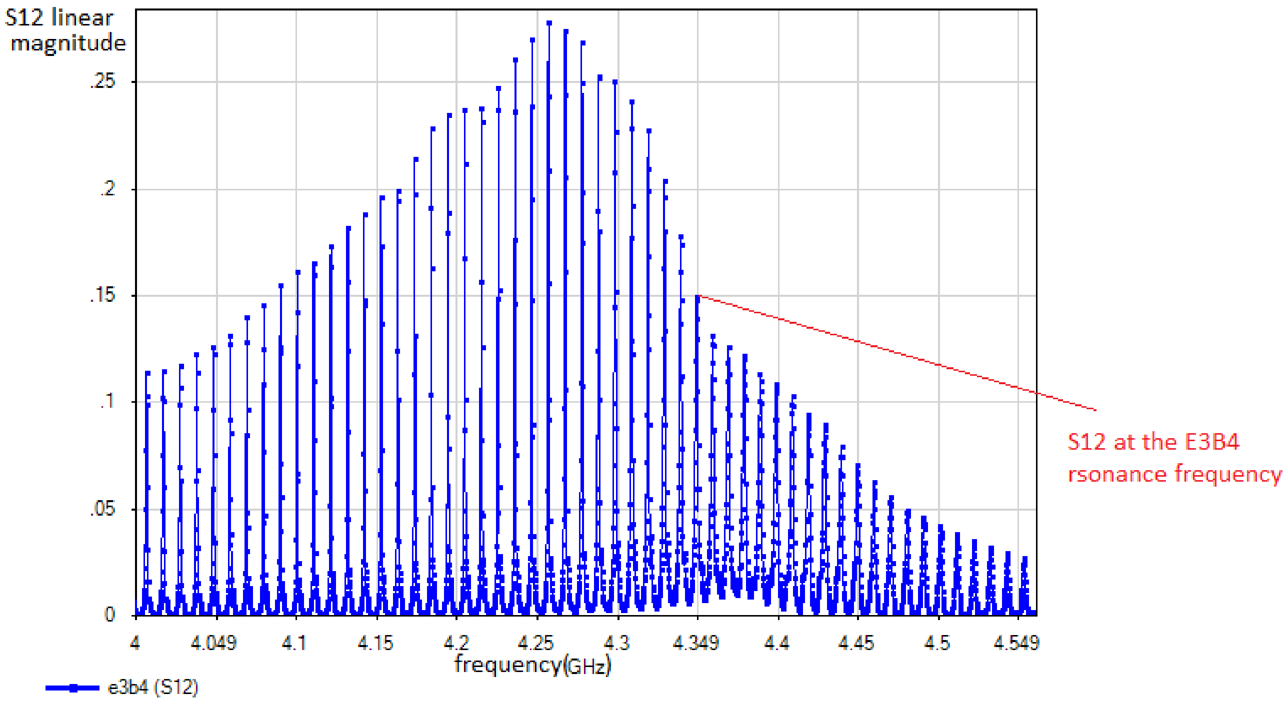

Figure 6.4: Transmission (S12) curve of the E3B4 resonator.

At the E3B4 resonance frequency ($f_r = 4.3488\ GHz$), we obtain:

$$S_{12} = |H| = 0.15 \tag{5.5}$$

H is the resonator transfer function at resonance frequency.

6.2.2 Amplifier

We suppose that G is the amplifier gain. As mentioned before, we need to have:

$$G * |H| = 1 \tag{5.6}$$

From the equations (5.5) and (5.6), we have that:

$$G = 6.7 = 16.52dB \tag{5.7}$$

6.2.3 Phase shifter

The phase shifter needs to validate the condition concerning the argument:

$$phase\ shift = -\arg(H) \tag{5.8}$$

We extract the argument of the transfer function at different frequencies from the S12 phase graph of the resonator (Figure 6.5).

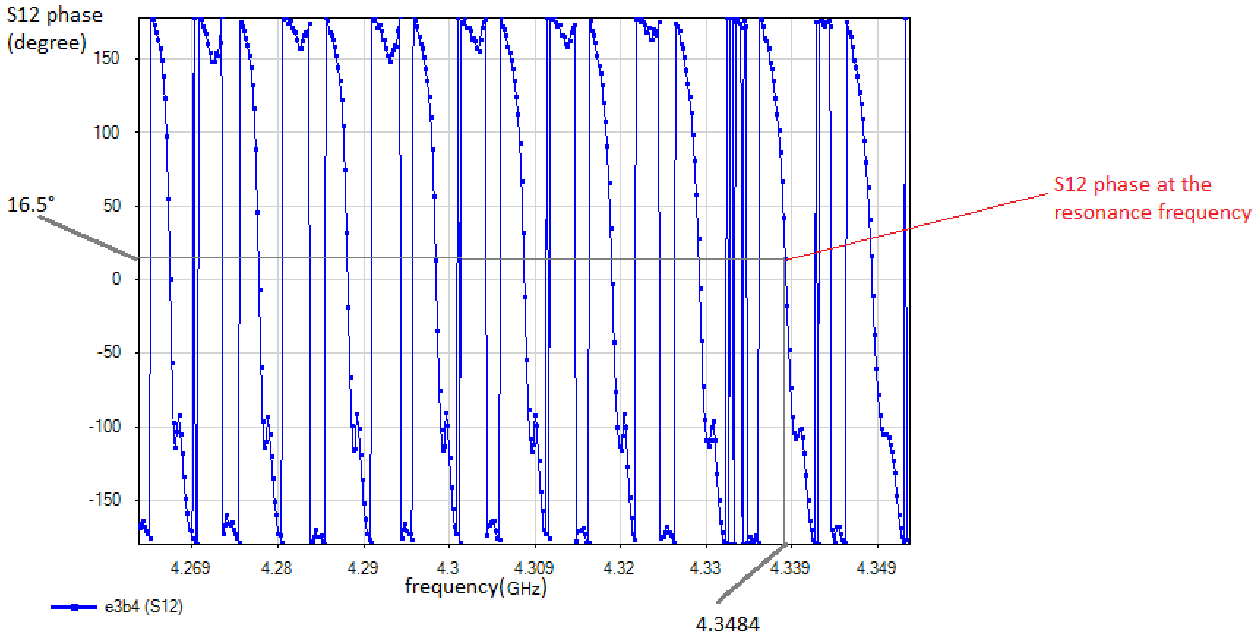

Figure 6.5 : S12 phase graph of the E3B4 resonator.

$$\arg\left(H(jW_r)\right) = 16.5\ deg \tag{5.9}$$

So

$$phase\ shift = -16.5\ deg \tag{5.10}$$

The phase shifter will be a transmission line without losses and with a characteristic impedance equal to 50Ω and an input impedance equal to 50Ω, so from the following equation(5.11) w conclude that the output impedance will be equal to 50Ω .

$$Z(l) = Z0 * \frac{Zi - jZ0\tan(\beta l)}{Z0 - jZi\tan(\beta l)}\ [\ 14\ ] \tag{5.11}$$

With Zi the input impedance and l the distance between in the line input and the point where we are measuring the impedance.

At this step, we have to define the length L with which the output wave of the transmission line (phase shifter) will have a phase delay φ, compared to the input wave, equal to 16.5 degrees. From the equations presented below we get a formula to make this calculation. By definition, we have that:

$$\varphi = \frac{2\pi}{\lambda} * L \tag{5.12}$$

$$L = \lambda * \frac{\varphi}{2 * 180} \tag{5.13}$$

In order to get concrete calculations, to calculate λ we need to define the transmission line material to get its ϵ_r to finish calculations. Therefore, we will choose FR-4 material, which is commonly used in such applications and have an ϵ_r equal to 4.3 so:

$$\lambda = 3.28\ \text{cm} \tag{5.14}$$

Consequently, we have:

$$l = 1.5\ mm \tag{5.15}$$

6.2.4 L1, L2 and L3 transmission lines

The L1 transmission line will have a length equal to $\frac{\lambda}{4} = 9.563\ mm$ and an input impedance $Z_{in} = Z_{11}(f_r) = Z_{22}(f_r)$ since the E3B4 resonator is symmetric. From the (Figure 6.6) we have that:

$$Y_{11} = \frac{1}{Z_{11}} = 0.02\ S \tag{5.16}$$

so:

$$Z_{in} = Z_{22}(4.3488GHz) = Z_{11}(4.3488GHz) \approx 50\Omega \tag{5.17}$$

As a consequence, using the equation (5.4), the characteristic impedance of the L1 transmission line will be equal to 50 Ω. For the same reason and with the same calculations, we could conclude that L2 and L3 transmission lines will be the same as L1.

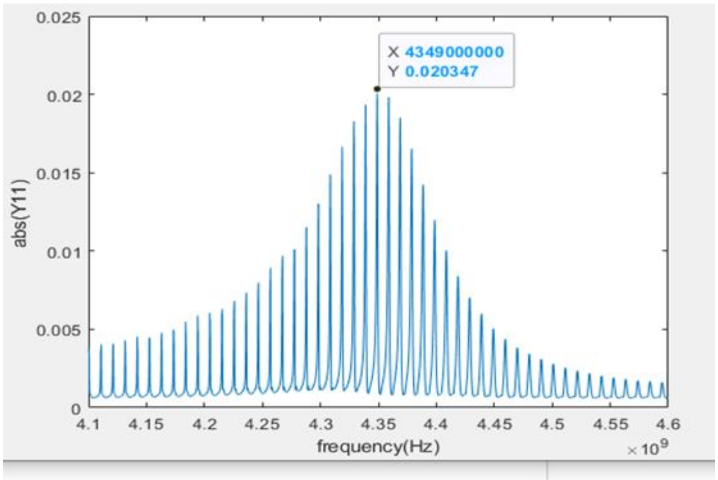

Figure 6.6 : The E3B4 resonator response

6.3 Central parameters for amplifier design

Since the motional resistance depends upon factors such as air gap between the resonator and electrodes, the coupling area… we could change it without changing the resonance and anti-resonance frequencies of the resonator.

Studying how the motional resistance affect the amplifier gain and the phase shifter length, will be useful for such design. Based on the resonator transfer function (obtained in chapter 2) and on the designed oscillator, we calculate the dependency graphs between motional resistance and amplifier gain (Figure 6.7). To do this, the resonator's electrical model parameters are fixed except the motional resistance (because we are just interested on the dependency graph and not exact values).

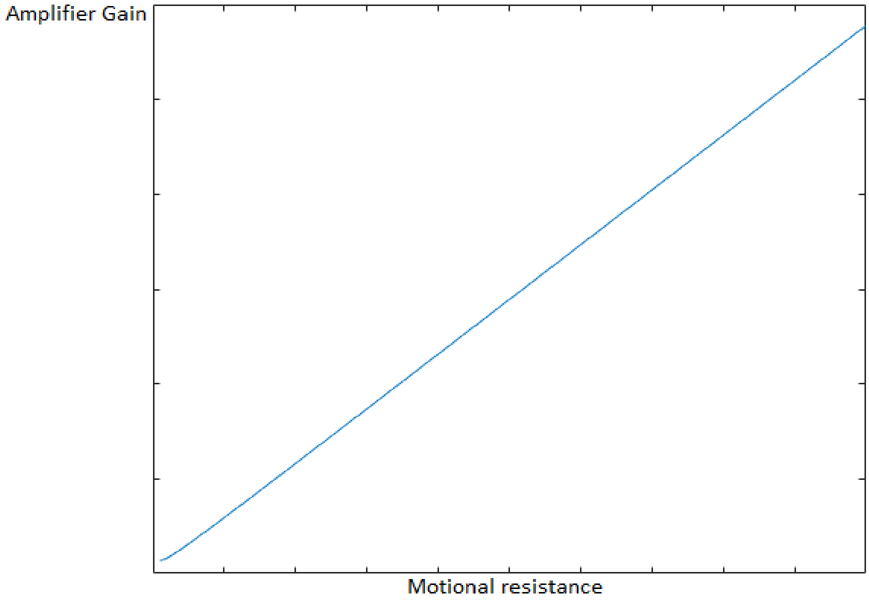

Figure 6.7 : The evolution of the amplifier gain as a function of the motional resistance.

The amplifier gain is proportional to the motional resistance. It is an expected result because the amplifier compensates the resonator insertion losses (the higher are insertion losses, the higher is the amplifier gain) and insertion losses are proportional to the motional resistance.

7 State of the art

Significant progress has been made in the last years to improve the performance of the radiofrequency oscillators for clock applications especially in their short time stability, which is related to their phase noise. In this chapter, we will start by performing a bibliographic study to find the “most” suitable MEMS resonator technology for timing applications, and compare it with the preliminary results presented in precedent chapters. We will start by defining the resonator’s parameters on which we will base our comparisons. Additionally, it is primordial to get an overview of existing oscillators, especially for 5G applications, in order to know if MEMS clocks can be a good alternative to these technologies or not.

7.1 Central parameters for characterizing MEMS resonators and oscillators adapted to 5G timing applications

In order to situate MEMS resonators and oscillators in the context of 5G applications, the first criteria is the resonator resonance frequency.

Clocks performances relies on their stability and phase noise. As seen in chapter 4, the resonator’s quality factor Q is the main phase noise contributor near the carrier frequency. In that case, high Q corresponds to low phase noise.

FKT/P0 term presented in chapter 4 and issued from Leeson’s equation, depends mainly on F, the noise figure of the amplifier (K and T are constants and P0 is the input power), and is proportional to the amplifier gain. From [1], we have that the higher is the motional resistance, the higher is the phase noise of the MEMS oscillator because of the higher gain sustaining amplifier is required. Since the phase noise far from the carrier frequency depends on FKT/P0 we conclude from what previously said that it depends on the motional resistance too.

7.2 Bibliographic study of MEMS resonators for timing applications

This part describes key findings from literature review and from previous work made in CEA-LETI to determine the state of the art of MEMS resonators for high frequency applications. As a first step in this bibliographic research, MEMS resonators are divided into groups according to their transduction mechanism (Figure 7.1).

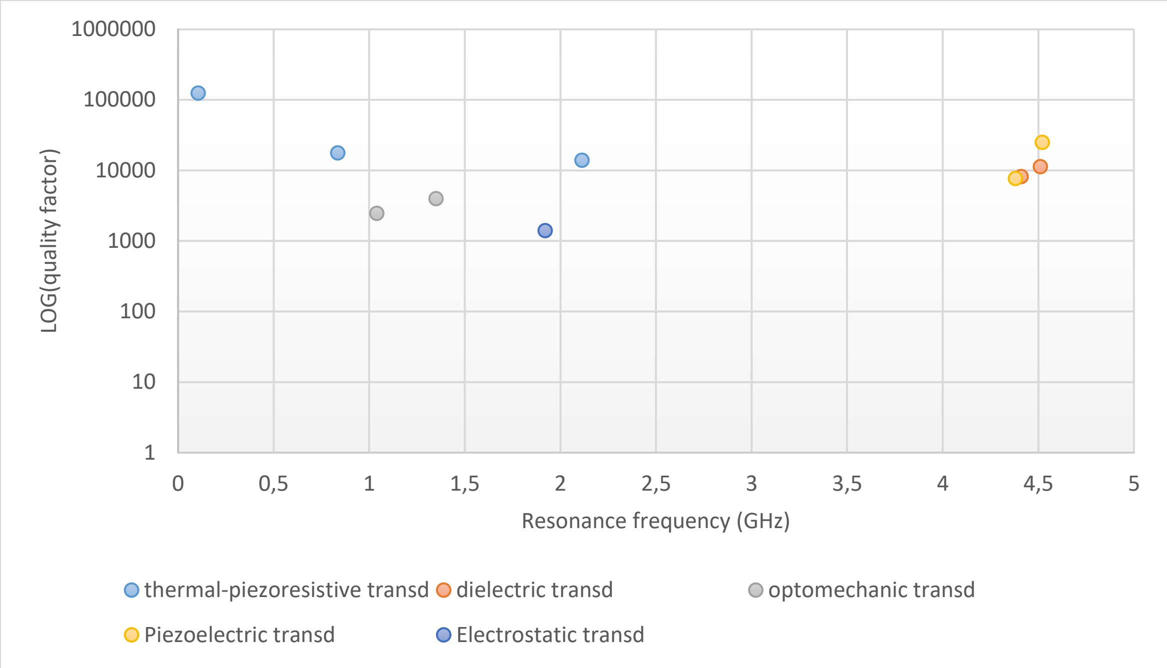

Figure 7.1 : Overview of different transduction technologies [19],[18],[17],[16],[15].

We distinguish that different works with piezoelectric transduction are successful to get a good trade-off, among them resonators of the ORAGE project *[31]* used in previous chapters. Therefore, as a next step in the study I focus on piezoelectric transduction. This technology can again be split into three main parts: Bulk Acoustic Wave resonators, Surface Acoustic Wave resonators and Lamb Wave resonators.

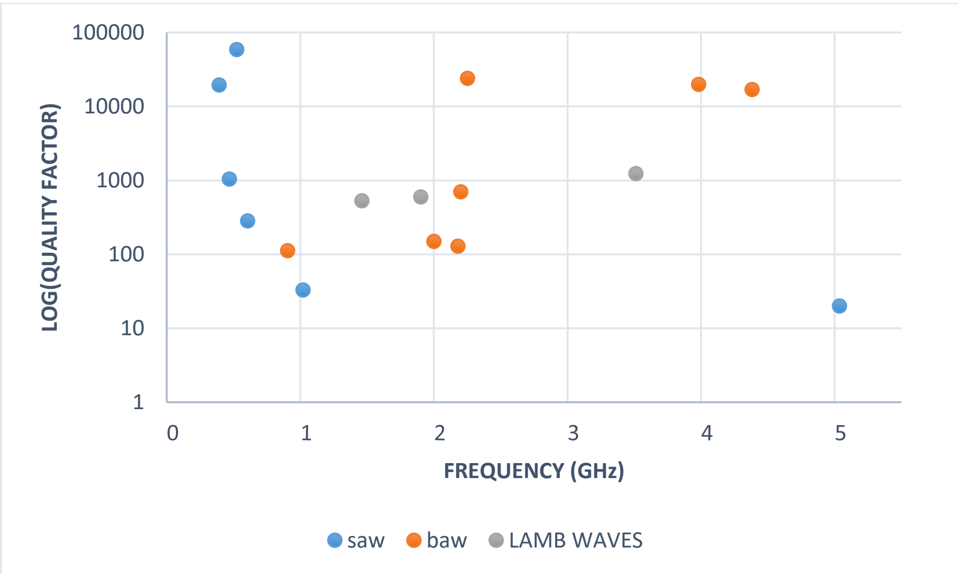

Figure 7.2 : Overview of SAW, BAW and lamb wave resonators, [25], [24],[23],[22],[21],[20]

BAW resonators represent, according to the graph above (Figure 7.2), a good technology that can be the starting point of the development of 5G clocks. We also find a high frequency SAW resonator [22] but with a low quality factor, that makes it inappropriate for such application.

I performed a further bibliographic investigation centered in BAW technology that ended with another split, between FBAR, HBAR and SMR resonators, presented in the graph below (Figure 7.3).

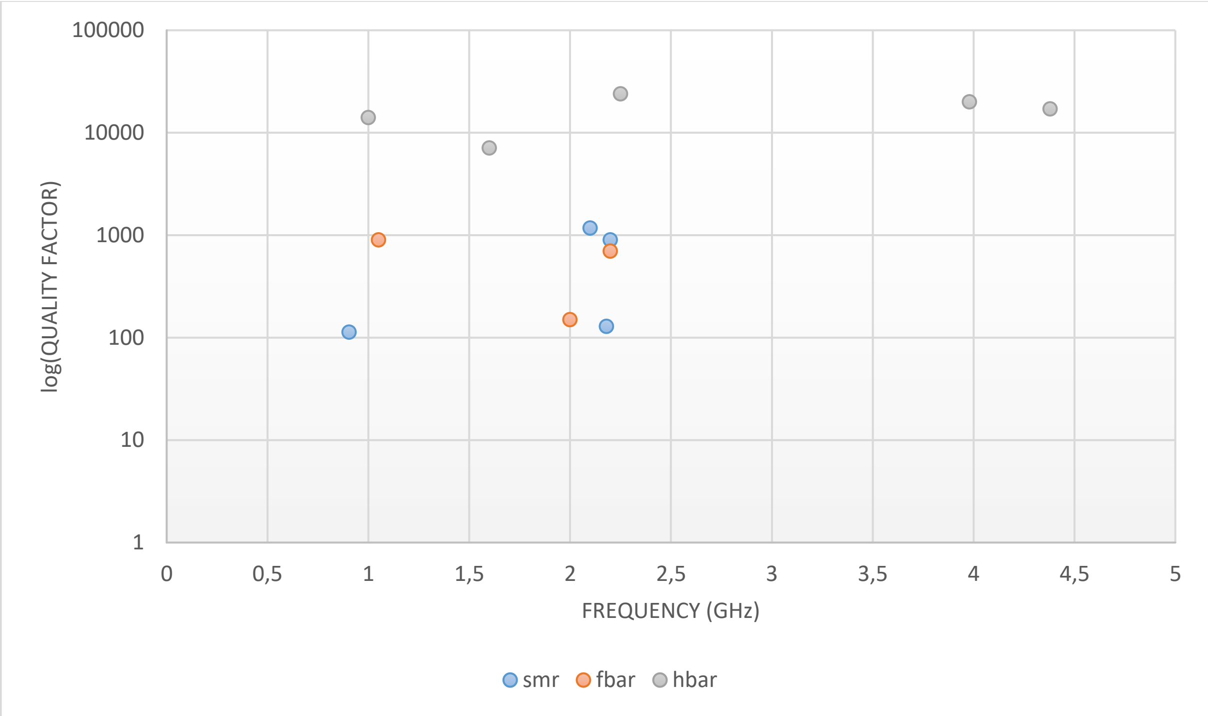

Figure 7.3 : Overview SMR VS FBAR VS HBAR, [27],[26],[31].

The previous figure shows a predominance of HBAR resonators over FBAR and SMR resonators in terms of quality factor and resonance frequency, But the quality factor does not give all the information about resonators performances: HBAR resonators have a huge insertion losses (high motional resistance) compared to other technologies, arising from the coupling mechanism. This makes it less than clear that they are good for clocks, or in any case they have to be carefully optimized,

7.3 Bibliographical study of oscillators: MEMS based and other existing technologies

There are mainly two different technologies of RF commercial oscillators: quartz oscillators and atomic oscillators. Atomic clocks are devices that use an internal resonance frequency of atoms (or molecules) to measure the passage of time. The three most commonly used ones for clocks are gas atoms: Cesium Cs, Rubidium Rb and hydrogen H. Their main characteristics are summarized in the Table 7-1 below. We have to note that these clocks are bulky and expensive, and as such they are mainly used in laboratories.

Table 7-1 : A summary of the different parts of the atomic clocks with a description of main characteristics, inspired from [38]

	Cesium	Rubidium	Hydrogen
Precision (per year)	2*10^(-11)	5*10^(-10)	
Working frequency	9.2GHz	6.835GHz	1.42GHz
Stability in temperature (interval)	5*10^(-11) (-28 to 65°C)	3*10^(-10) (-55 to 68°C)	
Stability (1second)	$5*10^{-11}$	$3*10^{-12}$	10^{-13}
Weight	10-20 kg	1.5-2.5 kg	
Power consumption	30 W	20W	140W

Quartz oscillators are more comparable to MEMS oscillators since they have almost same application domains. They consist of quartz crystal resonators and they can be classified into four main categories: XO, TCXO, OCXO, VCXO (Table 7-2).

Table 7-2 : A summary of the different parts of the quartz clocks with a description of main characteristics, inspired from [38]

	XO	TCXO	MCXO	OCXO
Precision (per year)	10-100ppm	2*10^(-8)	5*10^(-8)	10^(-8)
Stability in temperature (interval)	10-50 ppm	5*10^(-7) (-55 to 85°C)	3*10^(-8) (-55 to 85°C)	10^(-9) (-55 to 85°C)
Stability (1second)		10^{-8}	$3*10^{-10}$	10^{-12}
Weight	20g	50g	100g	200-500g
Power consumption	0.02W	0.04W	0.04W	0.6W

Table 7-3 shows a comparison between quartz and MEMS oscillators.

Table 7-3 : Comparison between MEMS and Quartz technologies in RF domain, inspired from [28].

	MEMS	Quartz
Size	√	
CMOS integration	√	
Packaging	√	
Temperature compensation	Almost the same	
Shock/vibration immunity	√	
Cost	Case-by-case	

Despite all advantages presented in MEMS devices, they have not yet displaced crystals oscillators since, in some specific applications, MEMS did not meet its predicted requirements. Adding to that, MEMS technology is relatively recent, as the first commercial timing products appeared in the last decade: therefore, quartz technology is better tested and understood.

To conclude what is concerning RF oscillators, Figure 7.4 is drawn mainly to show some examples of the best phase noise performance of the best phase noise performances of RF oscillators using different technologies and techniques.

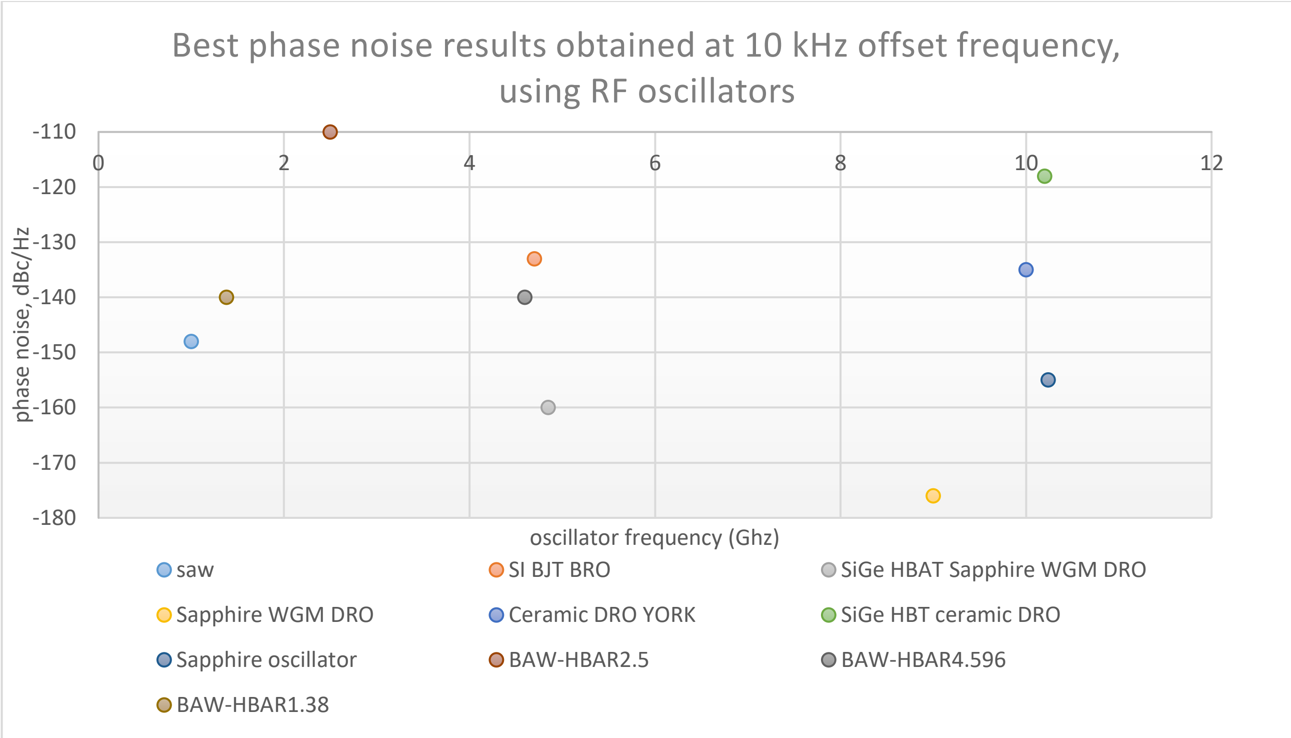

Figure 7.4 : Best phase noise results obtained at 10 KHz offset frequency, using RF oscillators [37],[36],[35],[34], [33], [32], [31],[30], [29].

Oscillators based on HBAR resonators, shows good stability and phase noise performances compared to other technologies oscillators. To make it a good alternative for existing RF oscillators, further work needs to be performed on HBAR technology to optimize the resonator (motional resistance quality factor and resonance frequency) and the closed loop components.

8 Conclusion

New communication standards in portable devices, such as the 5G technology, combine high carrier frequencies (up to tens of GHz) with narrow channel bandwidths. This requires time references (clocks) of increasing complexity, as they must present at the same time high frequencies, high performance (low phase noise), low cost and small power consumption. In this sense, MEMS time references present high frequency and small footprint. Over the last years, large research efforts have been put towards increasing their performance, and they are nowadays a commercial competitor to established technologies such as quartz.

During this internship, I performed the first steps towards the development of MEMS-based high-performance 5G clocks. During the first part of my internship I focused on the study on MEMS resonators. First I performed a general study of these devices, and in particular piezoelectric resonators: this gave me a broad overview of the field, and knowledge about the electrical equivalent models of these devices, which are important for the design of time references. Then I electrically characterized piezoelectric resonators fabricated in the CEA-LETI, in order to obtain their electrical equivalent parameters and main performance indicators, in order to choose the most promising devices. This allowed me to become familiarized with standard RF testing instruments, such as a probe station, a vector network analyzer and phase noise analyzer, which I was able to use autonomously at the end of my internship. During the second part of the internship I worked in MEMS time references, which comprise the resonator embedded in a feedback loop. First I studied the main performance indicators of reference oscillators, the jitter and phase noise. Then I analytically studied feedback loop configurations, and I designed a feedback loop specifically tailored to one of the measured devices. To finish my work, I performed a broad study of the state of the art in MEMS resonators, time references, and MEMS time references, by which I identified the most promising technologies for 5G applications. This study shows that HBAR (high-overtone bulk acoustic resonators) seem especially adapted for high-frequency low-noise applications, thanks to resonance frequencies of few GHz and high quality factors.

Future work will have to be performed in order to test the oscillator circuit that I designed, and experimentally verify its performance. A more complete study of HBAR devices will be necessary in order to verify that they can indeed comply with 5G specifications. More specifically, temperature stability is a key parameter in time references, which I have not studied during my internship.

9 References

[1]→ R. Abdolvand, B. Bahreyni, J. Lee, and F. Nabki, “Micromachined Resonators: A Review,” *Micromachines*, vol. 7, no. 9, p. 160, Sep. 2016.

[2]→ J. T. M. van Beek and R. Puers, “A review of MEMS oscillators for frequency reference and timing applications,” *J. Micromech. Microeng.*, vol. 22, no. 1, p. 013001, Jan. 2012.

[3]→ Lina, Liljelholm,. Electroacoustic evaluation of thin film piezoelectric resonators for frequency control and sensing applications,. Master, thesis (2005).

[4]→ Yoan, Civet,. Ajustement de la fréquence des résonateurs MEMS pour des applications de référence de temps,. PhD, thesis (2006).

[5]→ F. H. Villa-López, G. Rughoobur, S. Thomas, A. J. Flewitt, M. Cole, and J. W. Gardner, “Design and modelling of solidly mounted resonators for low-cost particle sensing,” *Meas. Sci. Technol.*, vol. 27, no. 2, p. 025101, Feb. 2016.

[6]→ T. Baron, E. Lebrasseur, F. Bassignot, G. Martin, V. Ptrini, and S. Ballandras, “High-Overtone Bulk Acoustic Resonator,” in *Modeling and Measurement Methods for Acoustic Waves and for Acoustic Microdevices*, M. G. Beghi, Ed. InTech, 2013.

[7]→ Thomas, Daugey., Jean-Michel, Friedt., Gilles, Martin., Rodolphe, Boudot. A HBAR-oscillator-based 4.596 GHz frequency source: Application to a
coherent population trapping Cs vapor cell atomic clock (2015)

[8]→ T. Baron, E. Lebrasseur, F. Bassignot, G. Martin, V. Ptrini, and S. Ballandras, “High-Overtone Bulk Acoustic Resonator,” in *Modeling and Measurement Methods for Acoustic Waves and for Acoustic Microdevices*, M. G. Beghi, Ed. InTech, 2013.

[9]→ A. J. Dickherber, C. D. Corso, and W. D. Hunts, “Development of Highly Sensitive Bulk Acoustic Wave Device Biosensor Arrays for Screening and Early Detection of Prostate Cancer:,” Defense Technical Information Center, Fort Belvoir, VA, Jan. 2009.

[10]→ D. B. Leeson, “Oscillator Phase Noise: A 50-Year Review,” *IEEE Trans. Ultrason., Ferroelect., Freq. Contr.*, vol. 63, no. 8, pp. 1208–1225, Aug. 2016.

[11]→ Walt, Kester,. Converting Oscillator Phase Noise to Time Jitter (2009).

[12]→ R. M. C. Mestrom, R. H. B. Fey, and H. Nijmeijer, “On phase feedback for nonlinear MEMS resonators,” in *2007 IEEE International Frequency Control Symposium Joint with the 21st European Frequency and Time Forum*, Geneva, Switzerland, 2007, pp. 765–770.

[13]→ F. He, R. Ribas, C. Lahuec, and M. Jézéquel, “Discussion on the general oscillation startup condition and the Barkhausen criterion,” Analog Integr Circ Sig Process, vol. 59, no. 2, pp. 215–221, May 2009.

[14]→ Ruzhdi, Sefa,. Arianit, Maraj,. Analysis of transmission lines matching using quarter-wave transformer (2011).

[15]→ D. Weinstein and S. A. Bhave, "PIEZORESISTIVE SENSING OF A DIELECTRICALLY ACTUATED SILICON BAR RESONATOR," in *2008 Solid-State, Actuators, and Microsystems Workshop Technical Digest*, Hilton Head, South Carolina, USA, 2008, pp. 368–371.

[16]→ A. Rahafrooz and S. Pourkamali, "High-Frequency Thermally Actuated Electromechanical Resonators With Piezoresistive Readout," *IEEE Trans. Electron Devices*, vol. 58, no. 4, pp. 1205–1214, Apr. 2011.

[17]→ X. Sun, K. Y. Fong, C. Xiong, W. H. P. Pernice, and H. X. Tang, "GHz optomechanical resonators with high mechanical Q factor in air," *Opt. Express*, vol. 19, no. 22, p. 22316, Oct. 2011.

[18]→ Sunil A. Bhave and Roger T. Howe,. INTERNAL ELECTROSTATIC TRANSDUCTION FOR BULK-MODE MEMS RESONATORS (2004)

[19]→ Dana, Weinstein,. GHz CMOS-MEMS resonators,. Seminar (2018).

[20]→ Y. Liu, D. Liu, S. Huang, Y. Li, L. He, and Y.-K. Chou, "A 20-Gb/s half-rate 4:1 multiplexer with multiphase clock architecture in 40-nm CMOS technology," in *2015 Asia-Pacific Microwave Conference (APMC)*, Nanjing, China, 2015, pp. 1–3.

[21]→ L. Shao *et al.*, "Phononic Band Structure Engineering for High- *Q* Gigahertz Surface Acoustic Wave Resonators on Lithium Niobate," *Phys. Rev. Applied*, vol. 12, no. 1, p. 014022, Jul. 2019.

[22]→ A. A. Md Ralib and A. N. Nordin, "SILICON COMPATIBLE ACOUSTIC WAVE RESONATORS: DESIGN, FABRICATION AND PERFORMANCE," *IIUMEJ*, vol. 15, no. 2, Nov. 2014.

[23]→ D. Neculoiu *et al.*, "AlN on silicon based surface acoustic wave resonators operating at 5 GHz," *Electron. Lett.*, vol. 45, no. 23, p. 1196, 2009.

[24]→ M. Narducci, M. Ferrari, V. Ferrari, and H. Campanella, "Aluminum Nitride SOI Lamb-wave Resonators towards Multi-frequency, Multi-sensitive Temperature Sensor Platform," *Procedia Engineering*, vol. 87, pp. 1152–1155, 2014.

[25]→ C. S. Lam, A. Gao, C.-M. Lin, and J. Zou, "A Review of Lamé and Lamb Mode Crystal Resonators for Timing Applications and Prospects of Lamé and Lamb Mode PiezoMEMS Resonators for Filtering Applications," p. 12.

[26]→ Wencheng, Xu,. Film Bulk Acoustic Resonators of High Quality Factors in Liquid Environments for Biosensing Applications,. PhD, Thesis (2011).

[27]→ : Humberto, Campanella,. Thin-film bulk acoustic wave resonators – FBAR,. PhD, Thesis (2007).

[28]→ : Bill, Schweber,. MEMS Oscillators Challenge Quartz Crystals in RF Applications (2014).

[29]→ Texas,Instruments., LMK05318 Ultra-Low Jitter Network Synchronizer Clock With Two Frequency Domains (2018)

[30]→ Thomas, Daugey., Jean-Michel, Friedt., Gilles, Martin., Rodolphe, Boudot. A HBAR-oscillator-based 4.596 GHz frequency source: Application to a
coherent population trapping Cs vapor cell atomic clock (2015)

[31]→ N. Chretien et al., “Double-port AlN/Sapphire high overtone bulk acoustic resonators for the stabilization of radio-frequency oscillators,” in 2012 IEEE International Ultrasonics Symposium, Dresden, Germany, 2012, pp. 2210–2213.

[32]→ Régis, M., Llopis, O., Van Haaren, B., Plana, R., Grhule, A., Rayssac, J. & Graffeuil, J.
Ultra-low phase noise C and X band bipolar transistor dielectric resonator oscillators.
Proc. IEEE Int. Freq. Contr. Symp., 507-511 (1998).

[33]→ Ivanov, E. N. & Tobar, M. E. Low phase noise sapphire crystal microwave oscillators:
current status. IEEE Trans. Ultrason. Ferroelect. Freq. Control 56, 263-269 (2009).

[34]→ Rohde, U., Poddar, A. & Calbaza, D. Searching for Low-Phase synthesizer. Microwave &
RF (2014).

[35]→ : Howe, D. A. & Hati, A. Low-noise X-band oscillator and amplifier technologies:
comparison and status. *Proc. IEEE Freq. Control Symp.*, 2005, Vancouver, BC, 481-487
(2005).

[36]→ : Cibiel, G. Contribution à l’analyse d’amplificateurs microondes à très faible bruit de phase:
application à la réalisation d’une source à très haute pureté spectrale en bande C. PhD
Thesis, Toulouse III, Paul Sabatier University, France (2003).

[37]→ : 26. Rohde, U., Poddar, A. & Calbaza, D. Searching for Low-Phase synthesizer. Microwave &RF (2014).

[38]→ Stephen R. Cantor, Avinoam, Stern,.Benny, Levy,. Clock Technology.

10 APPENDIX:

10.1 APPENDIX [A] :

```
clear all;
clc;

fmin=1.8e9; % %Minimum frequency sweep
fmax=2.5e9; %Maximum frequency sweep
deltaf_int=200e6; %frequency in which we calculate C0 and parasitic parameters
deltaf_fit=200e6; %fr intervall
nom_fichier_mesure='5eg13.s1p';%you have to put the name of the sXp file

[freq, s_Dut] = SXPParse(nom_fichier_mesure);%take the data from the sXp file as it is
y_Dut = s_to_y(s_Dut)/50;
y_Dut2(:)=y_Dut(1,1,:);%y_Dut(1,2;:) if we want to get Y12 for example
z_Dut = s_to_z(s_Dut)*50;
z_Dut2(:)=z_Dut(1,1,:);%z_Dut(2,1;:) if we want to get Z21 for example
moduleY=abs(y_Dut2);
moduleZ=abs(z_Dut2);
realY=real(y_Dut2);
imagY=imag(y_Dut2);
realZ=real(z_Dut2);
imagZ=imag(z_Dut2);
angleYdeg=rad2deg(angle(y_Dut2));
angleZdeg=rad2deg(angle(z_Dut2));
angleYrad=(angle(y_Dut2));
angleZrad=(angle(z_Dut2));

% An example of graphs that we can plot in the same frequency segment as declared in the VNA
%  plot(freq,realY);

%selection of the desirable frequency interval to make fitting or to graphs
%in that interval

ind_f_int=find(freq>fmin & freq<fmax);

freq_int=freq(ind_f_int);

moduleY_int=moduleY(ind_f_int);
moduleZ_int=moduleZ(ind_f_int);
realY_int=realY(ind_f_int);
imagY_int=imagY(ind_f_int);
realZ_int=realZ(ind_f_int);
imagZ_int=imagZ(ind_f_int);
angleYdeg_int=angleYdeg(ind_f_int);
angleZdeg_int=angleZdeg(ind_f_int);
angleYrad_int=angleYrad(ind_f_int);
angleZrad_int=angleZrad(ind_f_int);
```

10.2 APPENDIX [B]

```
%%parameters calculation for the fitting

ind_freq_fr_int=find(realY_int==max(realY_int));
ind_freq_fa_int=find(realZ_int==max(realZ_int));
fs_e=freq_int(ind_freq_fr_int);
fp_e= freq_int(ind_freq_fa_int);
Qs_e=abs((angleYrad_int(ind_freq_fr_int+1)-angleYrad_int(ind_freq_fr_int-1))/(freq_int(ind_freq_fr_int+1)-
freq_int(ind_freq_fr_int-1)))*fs_e/2;
Qp_e=abs((angleYrad_int(ind_freq_fa_int+1)-angleYrad_int(ind_freq_fa_int-1))/(freq_int(ind_freq_fa_int+1)-
freq_int(ind_freq_fa_int-1)))*fp_e/2;;
k2_e=pi/2*(fs_e/fp_e)/tan(pi/2*(fs_e/fp_e));
k2_e=pi.*pi./4.*((fp_e-fs_e)./fp_e).*fs_e./fp_e ;
C0_e=imag(y_Dut(1,1,1)/(2*pi*freq(1)));

Rs_e=min(realZ);
Ls_e=0.3e-9;
Cm_e=C0_e*((fp_e./1.2)^2/fs_e^2-1);
Lm_e=1/((2*pi*fs_e)^2*Cm_e);
Rm_e=1/(2*pi*fs_e*Qs_e*Cm_e);
R0_e=1/(2*pi*fp_e*Qp_e*Cm_e)-Rm_e;

Y_e_int=1./(1./(j*Cm_e*2*pi*freq_int)+Lm_e*j*2*pi*freq_int+Rm_e)+1./(1./(j*C0_e*2*pi*freq_int)+R0_e)
;%calculated from the MBVD model
Z_e_int=1./Y_e_int ;
%we could obtain now the results (graphs) of the MBVD model
moduleY_e_int=abs(Y_e_int);
angleYdeg_e_in=rad2deg(angle(Y_e_int));
moduleZ_e_int=abs(Z_e_int);
angleZdeg_e_int=rad2deg(angle(Z_e_int));
realY_e_int=real(Y_e_int);
realZ_e_int=real(Z_e_int);
Q_model=2*pi*fs_e*Lm_e/Rm_e; % the model quality factor
```

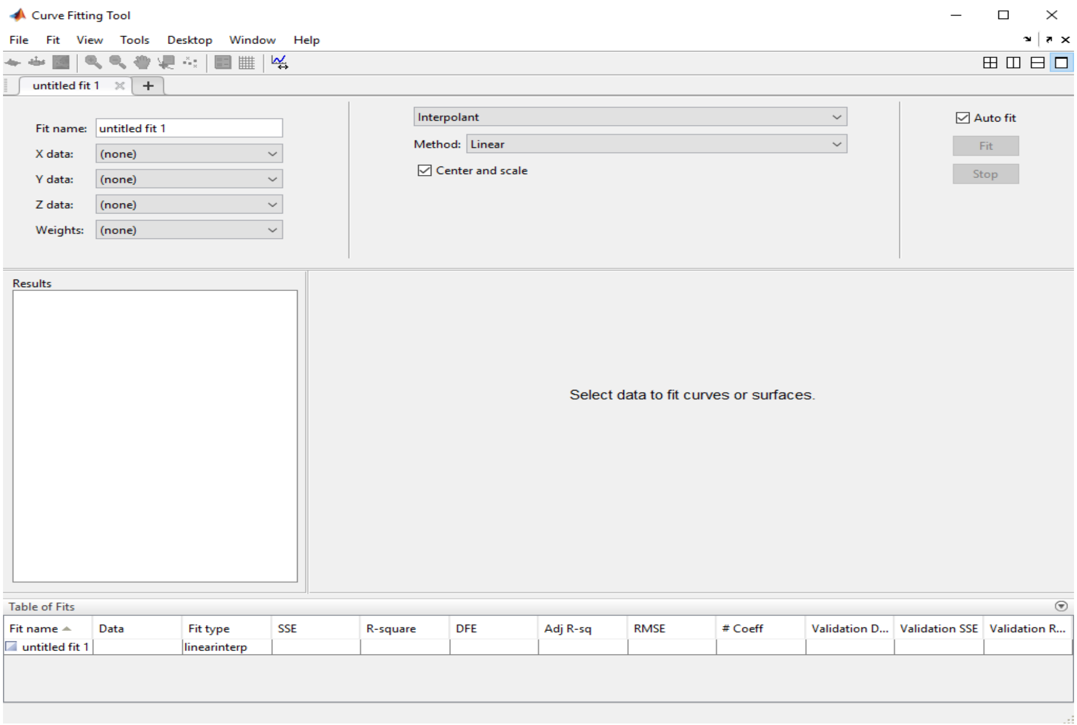

Figure 10.1 : Curve fitting tool used for optimizing electrical model parameters

10.3 APPENDIX [C]

```
import pyvisa

import time

import pandas as pd

rm=pyvisa.ResourceManager()

rm.list_resources()

instr = rm.get_instrument('GPIB0::17::0::INSTR')

instr.write('*IDN?')

print( instr.read())

instr.write('*RST')

instr.write('*CLS')

instr.write('INST:SEL PNO')

instr.write('INST:NSEL 20')

instr.write('CONF:PNO:MEAS SPEC')

instr.write('FREQ:CENT 2180MHz')

instr.write('FREQ:MULT 1')

instr.write('POW:RLEV -15')

instr.write('FREQ:STAR 300Hz')

instr.write('FREQ:STOP 30MHz')

instr.write('DISP:TRAC:Y:AUTO ON')

instr.write('INP:GAIN:AUTO ON')

instr.write('SPUR:SUPP NONE')

instr.write('INIT:CONT OFF')

instr.write('ABORT')

instr.write('INIT;*WAI;')

#time.sleep(35)

#to be confirmed

instr.write('FORM:DEXP:DSEP POIN')

instr.write('FORM:DATA ASC')

instr.write('TRAC? TRACE2')

data=instr.read()

instr.write('CALC:MARK1 ON')

instr.write('CALC:MARK2 ON')

instr.write('CALC:MARK3 ON')
```

```
instr.write('CALC:MARK1:TRAC 2')
instr.write('CALC:MARK2:TRAC 2')
instr.write('CALC:MARK3:TRAC 2')
instr.write('CALC:MARK1:X 1kHz')
instr.write('CALC:MARK2:X 1MHz')
instr.write('CALC:MARK3:X 20MHz')
instr.write('CALC:MARK1:Y?')
m1=instr.read()
#instr.write('CALC:MARK1:Y?')
#print( instr.read())
instr.write('CALC:MARK2:Y?')
m2=instr.read()
instr.write('CALC:MARK3:Y?')
m3=instr.read()
instr.write('DISP:TRAC:SPUR:HIGH OFF')
b=data.split(',')
f=b[::2]
bf=b[1::2]
liste_m = ['m1_1khZ', 'm2_1MHz', 'm3_20MHz']
l_m=[m1, m2, m3]
l1=['']*1399
l1[0]=liste_m[0]
l1[1]=liste_m[1]
l1[2]=liste_m[2]
l2=['']*1399
l2[0]=l_m[0]
l2[1]=l_m[1]
l2[2]=l_m[2]
df = pd.DataFrame.from_dict({'Frequence':f,'BruitPhase':bf,'marqueurs':l1,'valeurs':l2})
df.to_excel('mes_r2_2_18GHz.xlsx', header=True, index=False)
```